A 1 Reduction in Intact Cyanobacterial Photosystem I Particles Studied by Time-Resolved Step-Scan Fourier Transform Infrared Difference Spectroscopy and Isotope Labeling †

ARTICLE *in* BIOCHEMISTRY · MARCH 2005

Impact Factor: 3.02 · DOI: 10.1021/bi0497493 · Source: PubMed

3 AUTHORS, INCLUDING:

Velautham Sivakumar
University of Peradeniya
15 PUBLICATIONS **224** CITATIONS
SEE PROFILE

Gary Hastings
Georgia State University
56 PUBLICATIONS **1,106** CITATIONS
SEE PROFILE

A_1 Reduction in Intact Cyanobacterial Photosystem I Particles Studied by Time-Resolved Step-Scan Fourier Transform Infrared Difference Spectroscopy and Isotope Labeling†

Velautham Sivakumar, Ruili Wang, and Gary Hastings*

Department of Physics and Astronomy, Georgia State University, Atlanta, Georgia 30303

Received February 3, 2004; Revised Manuscript Received November 11, 2004

ABSTRACT: Time-resolved step-scan Fourier transform infrared (FTIR) difference spectroscopy, with 5 μs time resolution, has been used to produce $P700^+A_1^-/P700A_1$ FTIR difference spectra in intact photosystem I particles from *Synechococcus* sp. 7002 and *Synechocystis* sp. 6803 at 77 K. Corresponding spectra were also obtained for fully deuterated photosystem I particles from *Synechococcus* sp. 7002 as well as fully ^{15}N- and ^{13}C-labeled photosystem I particles from *Synechocystis* sp. 6803. Static $P700^+$/P700 FTIR difference spectra at 77 K were also obtained for all of the unlabeled and labeled photosystem I particles. From the time-resolved and static FTIR difference spectra, A_1^-/A_1 FTIR difference spectra were constructed. The A_1^-/A_1 FTIR difference spectra obtained for unlabeled trimeric photosystem I particles from both cyanobacterial strains are very similar. There are some mode frequency differences in spectra obtained for monomeric and trimeric PS I particles. However, the spectra can be interpreted in an identical manner, with the proposed band assignments being compatible with all of the data obtained for labeled and unlabeled photosystem I particles. In A_1^-/A_1 FTIR difference spectra obtained for unlabeled photosystem I particles, negative bands are observed at 1559 and 1549−1546 cm^{-1}. These bands are assigned to amide II protein vibrations, as they downshift ∼86 cm^{-1} upon deuteration and ∼13 cm^{-1} upon ^{15}N labeling. Difference band features at 1674−1677(+) and 1666(−) cm^{-1} display isotope-induced shifts that are consistent with these bands being due to amide I protein vibrations. The observed amide modes suggest alteration of the protein backbone (possibly in the vicinity of A_1) upon A_1 reduction. A difference band at 1754(+)/1748(−) cm^{-1} is observed in unlabeled spectra from both strains. The frequency of this difference band, as well as the observed isotope-induced shifts, indicate that this difference band is due to a 13^3 ester carbonyl group of chlorophyll *a* species, most likely the A_0 chlorophyll *a* molecule that is in close proximity to A_1. Thus A_1 reduction perturbs A_0, probably via a long-range electrostatic interaction. A negative band is observed at 1693 cm^{-1}. The isotope shifts associated with this band are consistent with this band being due to the 13^1 keto carbonyl group of chlorophyll *a*, again, most likely the 13^1 keto carbonyl group of the A_0 chlorophyll *a* that is close to A_1. Semiquinone anion bands are resolved at ∼1495(+) and ∼1414(+) cm^{-1} in the A_1^-/A_1 FTIR difference spectra for photosystem I particles from both cyanobacterial strains. The isotope-induced shifts of these bands could suggest that the 1495(+) and 1414(+) cm^{-1} bands are due to C⋯O and C⋯C modes of A_1^-, respectively.

Light absorption in photosystem I (PS I)[1] ultimately results in the generation of an electric potential gradient across the thylakoid membrane. This gradient is achieved by using light energy to transfer electrons across the membrane via a series of protein-bound pigment cofactors. In PS I the pigments are bound to two membrane-spanning protein subunits called PsaA and PsaB. Upon photoexcitation an electron is transferred from a specialized dimeric chlorophyll *a* (Chl-*a*) species called P700 to a nearby monomeric Chl-*a* acceptor called A_0 (*1*, *2*). The photogenerated radical pair is stabilized by further electron transfers: From A_0 an electron is transferred to A_1 [a phylloquinone (PhQ) molecule], then to F_X (an iron sulfur cluster), and then on to a set of iron sulfur clusters designated $F_{A/B}$ (*1*, *2*).

In PS I there are two symmetrical sets of cofactors bound to PsaA and PsaB (*3*, *4*), and below we will distinguish between them. For the phylloquinones (PhQs) bound to PsaA and PsaB we will call them A_{1-A} and A_{1-B}, respectively. Similarly, we will call the primary electron-accepting chlorophyll *a* cofactors A_{0-A} and A_{0-B}. Finally, we will refer to the pigments of P700 bound to PsaA and PsaB as P_A and P_B, respectively.

† This work was supported by the National Research Initiative of the USDA Cooperative State Research, Education and Extension Service, Grant No. 2004-35318-14889, to G.H.

* To whom correspondence should be addressed: phone 404-651-0748; fax 404-651-1427; e-mail ghastings@.gsu.edu.

[1] Abbreviations: A_{0-A}/A_{0-B}, primary electron acceptor in photosystem I bound to PsaA/PsaB; A_{1-A}/A_{1-B}, secondary electron acceptor in photosystem I bound to PsaA/PsaB; (B)Chl-*a*, (bacterio)chlorophyll *a*; C═O, carbonyl; C⋯O, semiquinone carbonyl; DFT, density functional theory; DS, difference spectrum(a) or spectroscopy(ic); ET, electron transfer; MQ, menaquinone; NQ, 1,4-naphthoquinone; $P_{A/B}$, chlorophylls of P700 bound to PsaA/PsaB; PS I, photosystem I; P700, primary electron donor in photosystem I; PBRCs, purple bacterial reaction centers; RT, room temperature; PhQ, phylloquinone (2-methyl-3-phytyl-1,4-naphthoquinone); RCs, reaction centers; *Rb*, *Rhodobacter*; *Rps*, *Rhodopseudomonas* (now known as *Blastochloris*).

10.1021/bi0497493 CCC: $30.25
Published on Web 01/20/2005

Recently it has been suggested that both sets of cofactors bound to PsaA and PsaB are involved in electron transfer (ET) in PS I from *Chlamydomonas reinhardtii* (*5*). This work motivated others to investigate the degree of directionality of the ET processes in PS I preparations from cyanobacteria (*6*, *7*). In both cyanobacterial and green algal PS I preparations at room temperature (RT), forward ET from A_1^- to F_X is characterized by time constants of 10−20 and 200−340 ns (see ref *7* for a recent review) that are thought to represent ET down either branch. The amplitudes of the two kinetic phases appear to be species-dependent and are ∼1:1 for *C. reinhardtii* (*5*) and 1:2−3 for cyanobacterial PS I (*7*). ET thus appears to be more unidirectional in cyanobacterial PS I.

Currently, it appears to be accepted that the 200−340 ns phase is associated with ET from A_{1-A}^- to F_X in all species (*7*), although there still remain questions as to how A_{1-A}^- is populated (*8*).

In cyanobacterial PS I particles from *Synechocystis 6803*, both the fast and slow phases are observable at low temperature. The fast phase is temperature-independent (*8*), while the slow phase shows a pronounced slowing as the temperature is decreased, with an activation energy of 110−220 meV (*8*, *9*). The slow phase, which is due to forward ET from $P700^+A_1^-$, is replaced by a $P700^+A_1^-$ recombination reaction as the temperature is lowered (*9*, *10*). At 77 K, in PS I particles from *Synechococcus elongatus*, $P700^+A_1^-$ recombination occurs with a lifetime (1/e) of ∼245 μs in ∼45% of the particles (*9*). The latter reaction pathway is crucial for the generation of a $P700^+A_1^-/P700A_1$ FTIR difference spectrum (DS): With a lifetime of ∼245 μs, the $P700^+A_1^-$ state is very difficult to photoaccumulate and is therefore very difficult to study by static FTIR difference spectroscopic (DS) techniques. Nanosecond (ns) and microsecond (μs) time-resolved step-scan (TRSS) FTIR DS techniques have been developed, allowing the acquisition of FTIR DS associated with short-lived transient intermediates (*11*−*14*). Due to dynamic range limitations inherent in fast (ns) electronics, ns TRSS FTIR DS is considerably less sensitive than μs TRSS FTIR DS. This is an important point, because in order to generate reliable TRSS FTIR DS for PS I, difference signals close to 10^{-5} (in OD units) need to be resolved (*13*). At present, it is not possible to reach this level of sensitivity with ns TRSS FTIR DS. However, it is possible with 5 μs TRSS FTIR DS. So if the transient species of interest can be made to decay on a time scale longer than 5 μs, highly sensitive TRSS FTIR DS associated with the transient species can be obtained. Since the $P700^+A_1^-$ state decays in ∼245 μs in cyanobacterial PS I at 77 K, it is then possible to obtain highly accurate $P700^+A_1^-/P700A_1$ FTIR DS by use of TRSS FTIR instrumentation with 5 μs time resolution at 77 K.

In this paper we have used 5 μs TRSS FTIR DS to produce $P700^+A_1^-/P700A_1$ FTIR DS. By also collecting static $P700^+$/P700 FTIR DS, we were then able to construct A_1^-/A_1 FTIR DS. We have obtained A_1^-/A_1 FTIR DS for trimeric cyanobacterial PS I particles from both *Synechococcus* sp. 7002 (*S. 7002*) and *Synechocystis* sp. 6803 (*S. 6803*). We have also obtained A_1^-/A_1 FTIR DS uniformly deuterated PS I particles from *S. 7002* and uniformly ^{15}N- and ^{13}C-labeled PSI particles from *S. 6803*. The observed isotope-induced band shifts allow a first assignment of IR difference bands to molecular modes of A_1, A_1^-, and its binding site.

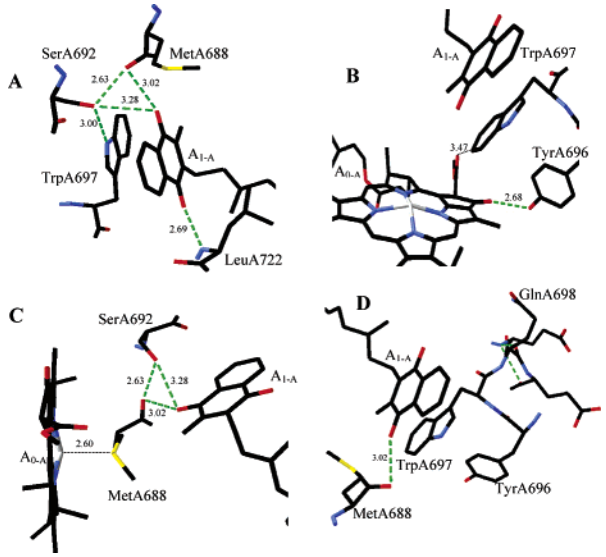

FIGURE 1: (A−D) Several views of A_{1-A} and its immediate protein environment. Possible H-bonding interactions of the PhQ carbonyls with the protein are shown as dotted lines. In part C, A_{0-A} and its environment are also shown. The B-side binding site is very similar. Figures were generated by Swiss PDBViewer (*15*) from the crystallographic coordinates of PS I at 2.5 Å resolution (*3*, *4*) [PDB file accession number 1JB0].

Structure of the A_1 Binding Site. Figure 1 shows several views of A_{1-A} and its binding site. The B-side binding site is very similar. The indole ring of TrpA697[2] is π-stacked upon A_{1-A}, with the ring planes being almost parallel (Figure 1A,B,D). The hydroxyl oxygen of SerA692 is 2.63 Å from the backbone oxygen of MetA688, 3.00 Å from the indole nitrogen of TrpA697, and 3.28 Å from the carbonyl oxygen of A_{1-A} that is adjacent to the methyl group (Figure 1A).[3] Given the geometry of SerA692, TrpA697, and MetA688, SerA692 is most likely H-bonded to the backbone of MetA688. The backbone oxygen of MetA688 is also 3.02 Å from one of the C═O oxygens of A_{1-A}. The carbonyl oxygen of A_{1-A} adjacent to the phytyl chain is H-bonded to the backbone amide nitrogen of LeuA722 (Figure 1A). The MetA688 sulfur atom ligates the central magnesium atom of A_{0-A} (Figure 1C). The hydroxyl oxygen of TyrA696 is 2.68 Å from the 13^1 keto C═O of A_{0-A} (Figure 1B). The 13^3 ester carbonyl oxygen of A_{0-A} is 3.47 Å from the closest carbon on the ring of TrpA697. It is also 3.51 Å from a carotenoid (not shown). GlnA698, GluA699, and GluA702 are also in close proximity to A_{1-A} (Figure 1D). The carbonyl oxygen of A_{1-A} adjacent to the methyl group is 8.97 Å from the 13^1 keto carbonyl oxygen of A_{0-A} and 8.28 Å from the 13^3 ester carbonyl oxygen of A_{0-A}. For comparison, in purple bacterial reaction centers (RCs) from *Rhodobacter sphaeroides*, the distance between the carbonyl oxygen of Q_A adjacent to the phytyl chain/methyl group and the 13^3 ester carbonyl oxygen of Bpheo-*a* is 10.16/11.22 Å (obtained from the crystal structure 1K6L).

[2] Throughout this paper we will use the *S. elongatus* amino acid numbering scheme rather than the *S. 7002* or *S. 6803* numbering scheme.

[3] Distances between atoms are given in angstroms to two significant figures. These distances were obtained by use of Swiss PDBviewer to analyze the deposited crystallographic coordinates (1JB0) (*3*−*4*). The actual resolution derived from the diffraction data is only 2.5 Å.

MATERIALS AND METHODS

Purified trimeric PS I particles from *Synechococcus* sp. PCC 7002 (*S. 7002*) were prepared as described previously (*16*). Cells were grown in H_2O or D_2O (>99.8%) growth media. All chemicals added to D_2O-based media were nondeuterated. D_2O incorporation into PS I particles from *S. 7002* was estimated to be ~98% by monitoring the amide II absorption band (Figure 6).

Monomeric and trimeric PS I particles from *Synechocystis* sp. 6803 (*S. 6803*) were prepared as described previously (*17*, *18*), from a mutant that lacks PS II. In our lab this mutant is grown photoheterotrophically in the presence of 5 mM glucose. For uniform ^{13}C labeling of cells, fully ^{13}C-labeled glucose (Isotec Inc.) was used in the growth medium. The extent of incorporation of the ^{13}C label was estimated to be >98% by monitoring the shift in the amide II absorption band (Figure 6). Similar estimates were also obtained by comparing photoaccumulated $P700^+$/P700 FTIR DS obtained for unlabeled and ^{13}C-labeled PS I particles at RT (data not shown). Uniformly ^{15}N-labeled PS I particles were prepared from cells that had been grown in the presence of ^{15}N-labeled nitrate, as described (*19*). In this paper we used monomeric ^{15}N- and ^{13}C-labeled PS I particles from *S. 6803*.

All static and time-resolved FTIR DS reported here were recorded on a Bruker IFS/66 spectrometer equipped with a fast, preamplified mercury−cadmium−telluride (MCT) detector (Graseby, D313). PS I samples were pelleted and placed between two circular 1-in. CaF_2 windows. Approximately 20 mM ascorbate and 10 μM phenazine methosulfate (PMS) were added to the pellet.

For TRSS FTIR DS experiments, laser pulses at 532 or 700 nm were used. Excitation (532 nm) was provided by a Nd:YAG laser (Model SL404G, Spectron Laser Systems, Rugby, England) and 700 nm excitation was obtained by use of a 532 nm pumped optical parametric oscillator (Integra OPO-C-532, GWU−Lasertechnik GmbH, Erftstadt-Freisheim, Germany) that is mounted on the invar support rods inside the Nd:YAG laser. TRSS FTIR DS obtained with either excitation wavelength were very similar. In the studies undertaken here, very low excitation intensities were used (0.8−1.5 mJ/pulse in a spot of diameter ~1 cm). At this level of excitation we do not observe any heating-induced artifacts in the TRSS FTIR DS taken at 77 K. Since spectra collected with either 532 or 700 nm excitation wavelengths are similar, in the following we will describe spectra obtained that are the average of spectra obtained with 532 or 700 nm excitation.

Before the sample was cooled, IR absorption spectra and $P700^+$/P700 FTIR DS were recorded. For all measurements, the amide I absorption band was less than 0.8 OD unit at room temperature, and the photoaccumulated FTIR difference bands in the 1800−1200 cm^{-1} region were of the correct shape and intensity (*19*). For static FTIR DS, the detector was AC-coupled.

The sample was then placed in a helium gas-flow cryostat (APD Cryogenics) and cooled to 77 K, and static $P700^+$/P700 FTIR DS were recorded prior to time-resolved measurements. For all static FTIR DS measurements, a 20 mW, helium−neon laser was used for light excitation. Sixty-four interferograms were collected before, during, and after light excitation. The spectra collected before illumination were ratioed directly against the spectra collected during and after illumination, as described (*19*, *20*). For static and time-resolved measurements, double-sided interferograms were collected at 4 cm^{-1} resolution. A Blackman-Harris three-term apodization function was used with a zero-fill factor of 2.

For TRSS FTIR DS measurements, the IR beam was filtered through two 1000−2000 cm^{-1} band-pass filters. One was placed before the sample while the other was placed directly in front of the detector. The later filter prevents actinic laser light (532 nm) from reaching the detector. Spectra were collected in the 2105−1060 cm^{-1} region at 4 cm^{-1} resolution. This requires sampling the interferogram 946 times (946 steps in the step-scan measurement). At each step the result of 20 laser flashes are averaged or coadded, so each step-scan experiment requires 18 920 laser flashes. At 10 Hz flash repetition rate this requires greater than 31.5 min. Each step-scan run was repeated 20−50 times on one sample and the results from at least three different samples were averaged. Therefore, the spectra shown here represent ~31.5−78.75 h of signal averaging at 10 Hz.

For TRSS FTIR DS measurements, the detector was DC-coupled and connected to a preamplifier with variable offset. The amplified signals were fed into a 200 kHz, 16-bit, analog-to-digital converter, thus limiting the time resolution to 5 μs. The lamp firing of the Q-switched YAG laser was used to synchronize the detection electronics to the laser pulse, and data collection was started ~135 μs prior to the laser flash. Data were collected in 5 μs increments and typically 200−400 data points were collected, resulting in data collection over 1−2 ms. Single-beam spectra collected prior to the laser flash (27 spectra) were averaged and then ratioed directly against all single-beam spectra collected (in 5 μs time intervals) after the laser flash. In this way transient absorption spectra were constructed. Opus 4.0 software from Bruker Optics was used for all spectral manipulations and calculations.

RESULTS

Figure 2 shows TRSS $P700^+A_1^-$/$P700A_1$ FTIR DS in the 1770−1270 cm^{-1} spectral region, obtained at 77 K for PS I particles from (A) *S. 7002* and (B) *S. 6803*. Each spectrum is the average of nine spectra collected in 5 μs increments. Clearly, even the decay of the weaker difference bands is discernible in the spectra. To show just how well resolved the difference bands in Figure 2 are, the time course of the absorption changes at several frequencies are shown in Figure 3. In Figure 3A the time course of the infrared (IR) absorption changes at 1938, 1754, 1748, and 1495 cm^{-1}, obtained following laser excitation of PS I from *S. 7002*, are shown. By fitting the four kinetics in Figure 3A simultaneously to a single-exponential component (plus a constant component), we find that the decays are characterized by a time constant (e^{-1}) of 262 μs. Figure 3B shows the time course of the IR absorption changes at 1754 and 1748 cm^{-1} for unlabeled and ^{15}N-labeled PS I particles from *S. 6803*. Upon ^{13}C labeling of PS I, the 1754 and 1748 cm^{-1} bands downshift to 1711 and 1704 cm^{-1} (see Figure 5A), respectively. The kinetics at 1711 and 1704 cm^{-1} for ^{13}C-labeled PS I from *S. 6803* are also shown in Figure 3B. By fitting the six kinetics in Figure 3B simultaneously to a

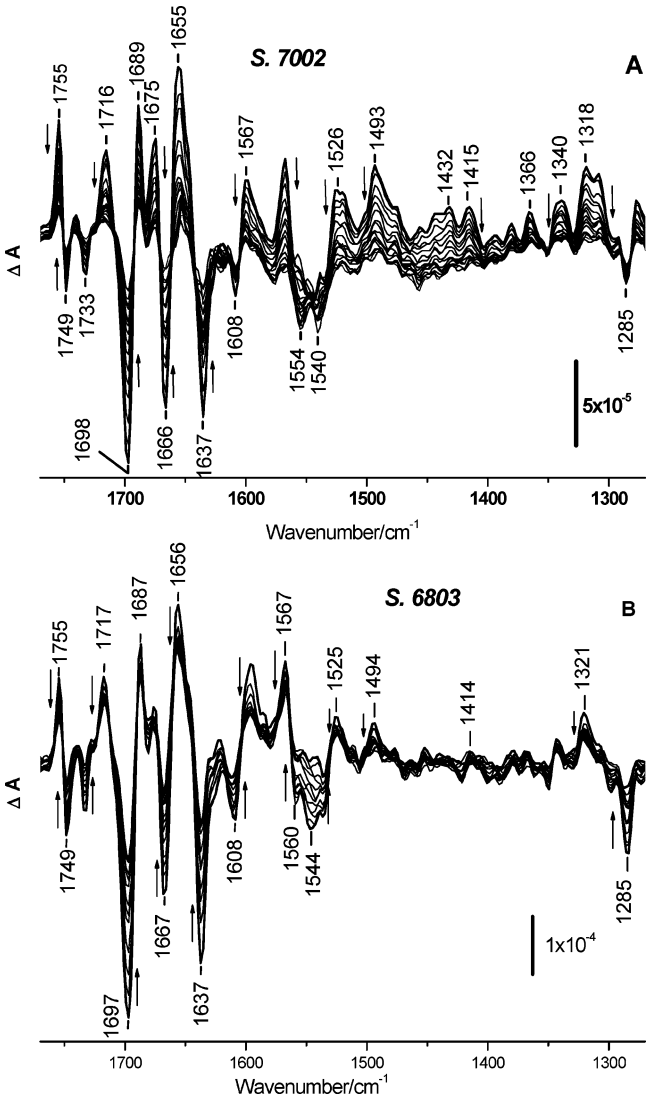

FIGURE 2: TRSS $P700^+A_1^-$/$P700A_1$ FTIR DS in the 1770−1270 cm^{-1} spectral region, obtained following laser excitation of (A) trimeric PS I particles from *S. 7002* and (B) monomeric PS I particles from *S. 6803* at 77 K. Each spectrum is the average of nine spectra collected in 5 μs increments. Thus each spectrum in the figure is separated by 45 μs. The *S. 7002* spectra are the average of 36 TRSS FTIR experiments on three samples. The *S. 6803* spectra are the average of 131 TRSS FTIR experiments collected with 532 or 700 nm excitation on four samples (79 TRSS FTIR experiments were performed with 700 nm excitation and 52 with 532 nm excitation). Within the noise, the spectra are identical whether 532 or 700 nm excitation was used (data not shown). The spectra shown with thicker lines represent the earliest and latest spectra after the laser flash. The arrows show the direction that the absorption bands move as time goes on.

single-exponential component (plus a constant component), we find that the decays are characterized by a time constant (e^{-1}) of 352 μs, which is slightly longer that found for PS I from *S. 7002*. The decay time constants for *S. 6803* and *S. 7002* agree well with the time constant of 245 μs ($t_{1/2}$ = 170 μs) obtained from previous pump−probe work on PS I from *S. elongatus* at 77 K (*9*). This is notable as the sample conditions for the FTIR and pump−probe experiments are quite different.

In Figure 3, all of the traces show absorption changes at single frequencies that are limited only by the instrumental resolution of 4 cm^{-1}. They have not been averaged over a frequency range in the same manner as described previously

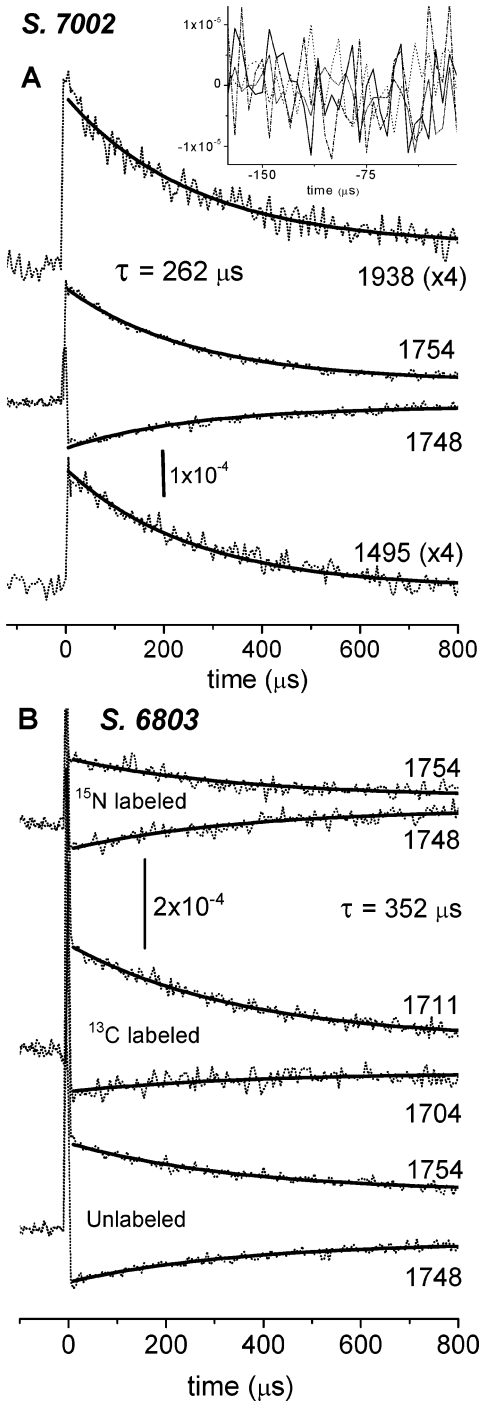

FIGURE 3: (A) Kinetics of absorption changes at 1938, 1754, 1748, and 1495 cm^{-1} obtained following 532 nm laser excitation of PS I particles from *S. 7002*. Data were collected in 5 μs increments. The four kinetics were fitted simultaneously to a single-exponential plus a constant. The fitted functions shown (solid lines) are characterized by a time constant of 262 μs. The 1938 and 1495 cm^{-1} kinetics (and their fitted functions) have been multiplied by 4 for ease of viewing. The inset shows the kinetic data collected prior to the laser flash (in this case the 1938 and 1495 cm^{-1} kinetics have not been multiplied by 4), which indicates a noise level of $\pm 1 \times 10^{-5}$. (B) Kinetics of absorption changes at 1754 and 1748 cm^{-1} following laser flash excitation of unlabeled (bottom) and ^{15}N-labeled (top) PS I particles from *S. 6803*. The kinetics at 1711 and 1704 cm^{-1} are also shown for ^{13}C-labeled (middle) PS I particles from *S. 6803*. Data were again collected in 5 μs time increments. The six kinetics were fitted simultaneously to a single-exponential plus a constant. The fitted functions are also shown (solid lines). The time constant obtained from the fitting procedure is 352 μs.

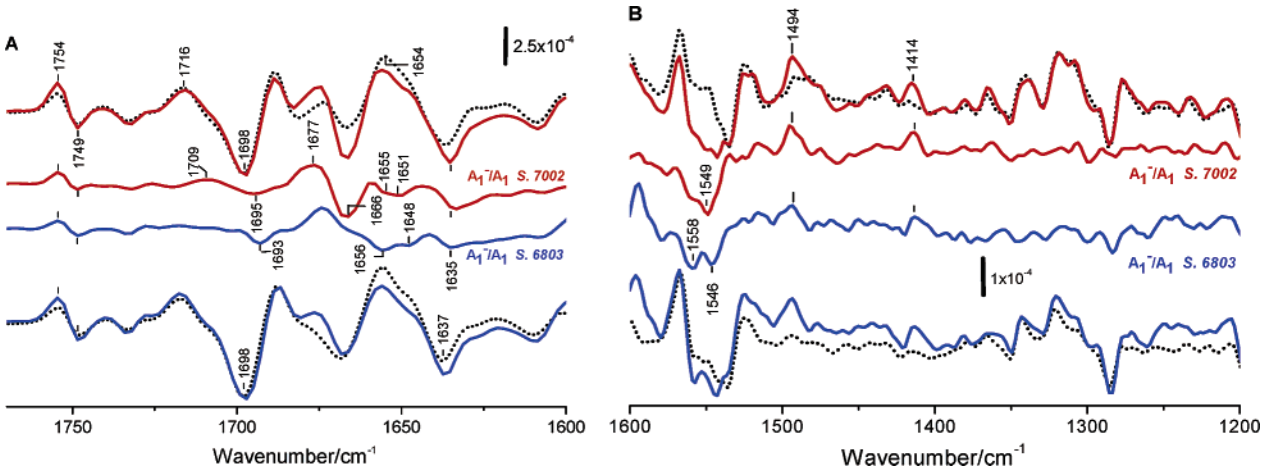

FIGURE 4: Static $P700^+/P700$ (dotted lines) and time-resolved $P700^+A_1^-/P700A_1$ (solid lines) FTIR DS in the (A) 1770−1600 and (B) 1600−1200 cm^{-1} spectral regions, obtained from trimeric PS I particles from *S. 7002* (top) or monomeric PS I particles from *S. 6803* (bottom) at 77 K. The time-resolved FTIR DS shown are the average of nine spectra, collected in 5 μs increments between 5 and 50 μs after the laser flash (the first spectrum after the laser flash in Figure 3). Subtraction of the static $P700^+/P700$ FTIR DS from the time-resolved $P700^+A_1^-/P700A_1$ FTIR DS results in the spectra that are labeled as A_1^-/A_1 FTIR DS.

(*21*). In addition, no baseline correction has been applied to any of the data in Figure 3. Only a few kinetic traces are shown in Figure 3. However, for each step-scan run, kinetics are obtained every 2.06 cm^{-1}, at over 500 frequencies. From the data collected prior to the laser flash (Figure 3A, inset) we find that the noise level in our experiments is roughly $\pm 1.0 \times 10^{-5}$ in optical density (OD) units.

For the kinetics in Figure 3B associated with unlabeled PS I, the absorption change at ~800 μs has an amplitude that is still ~50% of the amplitude of the initial absorption change (at ~45 μs). This means that in ~50% of the PS I particles longer-lived states, with lifetimes on a millisecond (or longer) time scale, are formed. In contrast, for the kinetics obtained for PS I particles from *S. 7002* (Figure 3A), the absorption change at ~800 μs after the laser flash has an amplitude that is only ~20% of the amplitude of the absorption change at ~5 μs. So it appears that the proportion of longer-lived states that contribute to the flash-induced absorption changes at 77 K is much higher in PS I from *S. 6803* compared to *S. 7002*. These longer-lived states are due to $P700^+F_X^-$ formation in a fraction of the PS I particles. From previous pump−probe work on PS I from *S. elongatus* at 77 K, it was found that $P700^+F_X^-$ could form in ~30% of the PS I particles and that it decayed with a lifetime of >5 ms (*9*).

In $P700^+/P700$ FTIR DS, a broad "roof-shaped" positive absorption band is found centered near 3200 cm^{-1} and extending over most of the 5000−1000 cm^{-1} region (*20*). This band is due to an electronic transition that reflects the dimeric nature of P700 (*20*, *22*). The 1938 cm^{-1} kinetic trace in Figure 3A therefore indicates the formation and decay of this electronic absorption band that is due only to $P700^+$. Similarly, P700 and $P700^+$ do not absorb greatly at 1495 cm^{-1}, and the kinetic at this wavelength is mostly due to the decay of A_1^-. The kinetic at 1754 cm^{-1} contains contributions that are associated with the decay of $P700^+$ and A_1^- while the kinetic at 1748 cm^{-1} contains contributions that are associated with the recovery of P700 and A_1 (see below).

Figure 4 shows the average of nine time-resolved $P700^+A_1^-/P700A_1$ FTIR DS, collected in 5 μs increments between 5 and 50 μs (the first spectrum after the laser flash in Figure 3), for PS I particles from *S. 7002* (top, solid line) and *S. 6803* (bottom, solid line) incubated in H_2O at 77 K.[4] Also shown in Figure 4 (dotted lines) are the static $P700^+/P700$ FTIR DS at 77 K, collected by standard photoaccumulation procedures (*19*, *23*). Subtracting the static spectra from the corresponding time-resolved spectra results in double difference spectra, which are labeled A_1^-/A_1 FTIR DS (middle two spectra) in Figure 4.

The $P700^+A_1^-/P700A_1$ and $P700^+/P700$ FTIR DS were normalized so that the 1716(+)/1698(−) cm^{-1} difference band has a similar amplitude in both spectra. This normalization also minimizes the differences in many of the bands in the spectra. For example, the broad absorption changes above 1800 cm^{-1} (not shown) or the 1285 cm^{-1} band, both of which are well-known marker bands for P700, are absent in the A_1^-/A_1 FTIR DS. The normalization applied implicitly assumes that the 1716(+)/1698(−) cm^{-1} difference band is due only to P700 and that modes of A_1 or other protein modes contribute negligibly. On the basis of FTIR spectra for quinones in vitro (*24*) and in purple bacterial RCs (*24*), this assumption is appropriate. Notice that the normalization procedure takes into account differences in the population of $P700^+$ that may contribute to the static and time-resolved FTIR DS. If this were not true, then all of the characteristic bands of P700 would show up in the A_1^-/A_1 FTIR DS. This clearly is not the case in our spectra.

Figure 5 shows the same A_1^-/A_1 FTIR DS that are shown in Figure 4 for unlabeled trimeric PS I particles from *S. 7002* (spectrum b) and monomeric PS I particles from *S. 6803* (spectrum d). In addition, A_1^-/A_1 FTIR DS that were obtained for unlabeled trimeric PS I particles from *S. 6803* (c) and ^{2}H-labeled (deuterated) trimeric PS I particles from *S. 7002* (a), as well as ^{15}N- (d) and ^{13}C- (e) labeled monomeric PS I particles from *S. 6803*, are shown.

In unlabeled *S. 6803* and *S. 7002* A_1^-/A_1 FTIR DS, a difference band is clearly observed at ~1755(+)/1749 cm^{-1}

[4] In this paper, we have averaged only the first nine spectra after the laser flash. Given that the kinetics display single-exponential behavior, we could have averaged spectra over a greater time window, to improve the signal-to-noise ratio in the spectra still further.

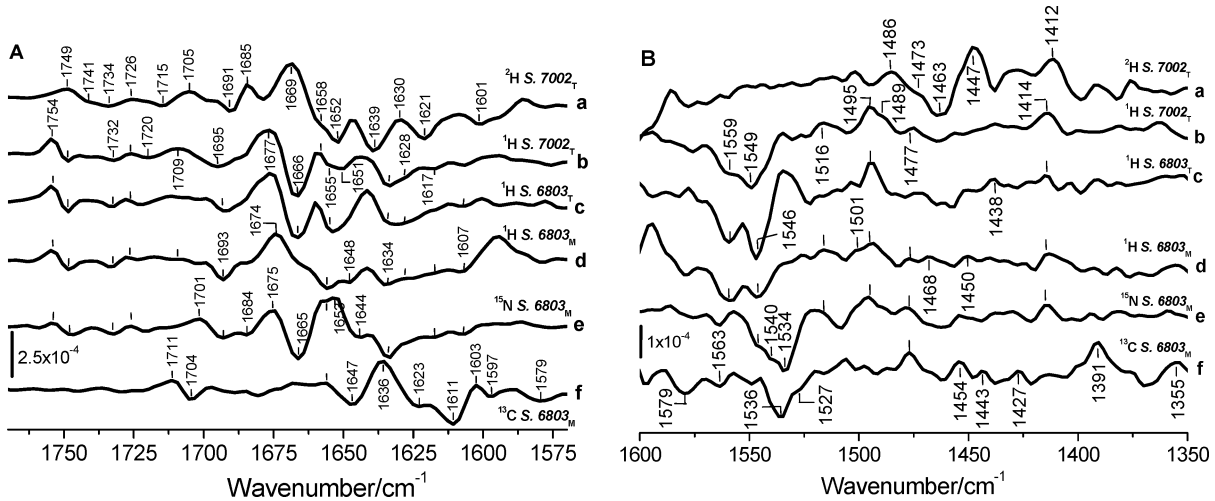

FIGURE 5: A_1^-/A_1 FTIR DS in the (A) 1770−1570 and (B) 1600−1350 cm^{-1} regions, obtained for (b) unlabeled and (a) deuterated trimeric PS I particles from *S. 7002*. The A_1^-/A_1 FTIR DS obtained for unlabeled trimeric (c) and monomeric (d) PS I particles from *S. 6803* are also shown, as are the spectra for ^{15}N- (e) and ^{13}C- (f) labeled monomeric PS I particles from *S. 6803*. All measurements were undertaken at 77 K. Spectra b and d are also presented in Figure 4.

(spectra b−d in Figure 5A). This difference band is unaffected by ^{15}N labeling and downshifts 44/45 cm^{-1} to 1711/1704 cm^{-1} upon ^{13}C labeling (Figure 5A). The corresponding difference band is found at 1749(+)/1743(−) cm^{-1} in the ^2H *S. 7002* A_1^-/A_1 FTIR DS, although the negative part of the difference band is quite poorly resolved. The kinetics at 1755 and 1749 cm^{-1} are shown in Figure 3A,B, demonstrating that the features at these frequencies are well resolved.

For unlabeled trimeric PS I particles from both *S. 6803* and *S. 7002*, the A_1^-/A_1 FTIR DS are very similar (spectra b and c in Figure 5A), displaying an intense difference band at 1677(+)/1666(−) cm^{-1}. A similar feature is observed at 1674(+)/1656(−) cm^{-1} in the monomeric ^1H *S. 6803* A_1^-/A_1 FTIR DS (spectrum d) and at 1636(+)/1611(−) cm^{-1} in the ^{13}C *S. 6803* A_1^-/A_1 FTIR DS (spectrum f). The details of how the above band shifts upon ^{15}N or ^2H labeling are discussed below. The differences between the A_1^-/A_1 FTIR DS obtained for unlabeled monomeric or trimeric PS I particles appears to result from the shift of an amide I mode in the different types of particles (see below).

In Figure 5B, intense negative features are observed at 1559 and 1549 cm^{-1} in the ^1H *S. 7002* A_1^-/A_1 FTIR DS. These features are completely absent in the ^2H *S. 7002* A_1^-/A_1 FTIR DS. Similar features are observed at 1559(−) and 1546(−) cm^{-1} in the ^1H *S. 6803* A_1^-/A_1 FTIR DS, at ∼1546(−) and 1534(−) cm^{-1} in ^{15}N *S. 6803* A_1^-/A_1 FTIR DS, and at ∼1536(−) and possibly 1527(−) cm^{-1} in ^{13}C *S. 6803* A_1^-/A_1 FTIR DS.

Positive bands are observed at 1495 and 1414 cm^{-1} in the unlabeled *S. 7002* and *S. 6803* A_1^-/A_1 FTIR DS. Similar bands at the same frequency are also observed in ^{15}N *S. 6803* A_1^-/A_1 FTIR DS. Corresponding bands probably appear at 1486 and 1412 cm^{-1} in the ^2H *S. 7002* A_1^-/A_1 FTIR DS. The 1495 cm^{-1} band in unlabeled spectra could appear at 1477 or 1454 cm^{-1} in the ^{13}C *S. 6803* A_1^-/A_1 FTIR DS.

Figure 6 shows representative IR absorption spectra in the 1800−1400 cm^{-1} region (amide I and II region) for unlabeled (a) and ^{15}N- (b) and ^{13}C- (d) labeled PS I particles from *S. 6803*. The IR absorption spectrum for ^2H-labeled PS I particles from *S. 7002* is also shown (c). The IR absorption

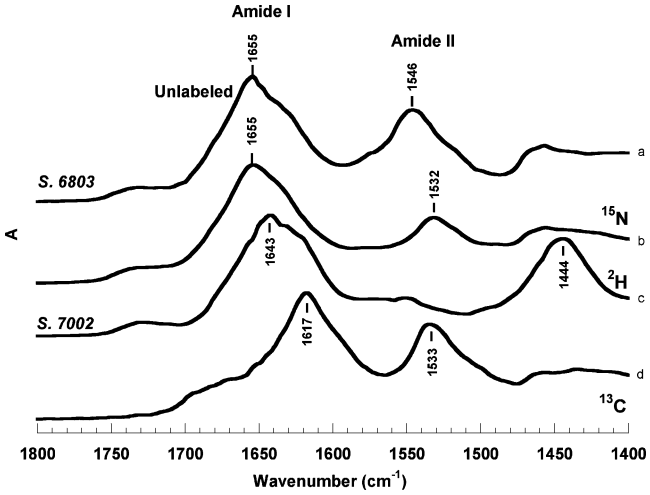

FIGURE 6: IR absorption spectra for unlabeled (a), ^{13}C-labeled (d), and ^{15}N-labeled (b) monomeric PS I particles from *S. 6803*. The IR absorption spectrum for ^2H-labeled trimeric PS I particles from *S. 7002* is also shown (c). The IR spectra for unlabeled PS I particles from *S. 7002* and *S. 6803* are virtually identical. For all of the labeled PS I particles, isotope incorporation is ∼98%. All spectra shown were obtained at RT.

spectrum for unlabeled PS I from *S. 7002* is virtually identical to spectrum a. Upon $^2H/^{15}N/^{13}C$ labeling, the amide I absorption band downshifts ∼12/0/38 cm^{-1} while the amide II absorption band downshifts ∼102/14/13 cm^{-1}, respectively. These isotope shifts are useful for determining if bands in FTIR DS are due to amide I or II modes (see below).

DISCUSSION

Species That Can Give Rise to Bands in Static and Time-Resolved FTIR DS at 77 K. Upon light excitation of cyanobacterial PS I particles from *S. elongatus* at 77 K, several processes occur. It is likely that similar processes also occur in cyanobacterial PS I from *S. 6803* and *S. 7002* (see below). First, in ∼35% of the RCs, P700 is irreversibly oxidized (*9*). These RCs do not contribute to either the static or the time-resolved FTIR DS. In a second portion of RCs (∼45%), ET from A_1^- to F_X is inhibited, and the $P700^+A_1^-$

state recombines in ~245 μs (*9*). Given such a short lifetime, it would be very difficult to photoaccumulate any significant population of this species. Thus it is unlikely that the $P700^+A_1^-$ state contributes appreciably to bands in photoaccumulated (static) FTIR DS. The $P700^+A_1^-$ state will only contribute to microsecond time-resolved FTIR DS. In a third portion of RCs (~20%), the $P700^+F_X^-$ state has a lifetime in the 5−100 ms range (*9*). Given this lifetime, it is the $P700^+F_X^-$ state that will be predominantly photoaccumulated. Thus the static FTIR DS is predominantly due to the $P700^+F_X^-$ state. The $P700^+F_X^-$ state will also contribute to time-resolved FTIR DS, and at times greater than ~800 μs, this state will be the dominant contributor to the time-resolved FTIR DS.

In summary, at 77 K, the static FTIR DS is due to $P700^+F_X^-$ formation while the time-resolved FTIR DS is due to $P700^+A_1^-$ formation. We will call these spectra $P700^+A_1^-/P700A_1$ and $P700^+F_X^-/P700F_X$ FTIR DS, respectively. By subtracting the $P700^+F_X^-/P700F_X$ far-IR DS from the $P700^+A_1^-/P700A_1$ FTIR DS, in a way that minimizes contributions from bands of P700 and $P700^+$ in the resultant spectrum, an $A_1^-F_X/A_1F_X^-$ FTIR DS can be constructed. On the basis of $P700^+/P700$ FTIR DS collected at room temperature (RT), it is well established that F_X^- and F_X do not contribute to $P700^+/P700$ FTIR DS in the 2000−1000 cm^{-1} region (*23*). It seams likely that this will also be the case at 77 K. F_X itself is not expected to display any absorption bands in the 2000−1000 cm^{-1} region, although we cannot entirely rule out the possibility that protein modes near F_X could contribute to our TRSS FTIR DS at 77 K. Previous photoaccumulated $P700^+F_X^-/P700F_X$ FTIR DS, obtained for PS I particles from *S. 6803* at 90 K, could not relate any difference bands to protein modes perturbed by F_X^- formation, and the spectra obtained were simply referred to as $P700^+/P700$ FTIR DS (*22*). Similarly, we will refer to the $A_1^-F_X/A_1F_X^-$ FTIR DS as A_1^-/A_1 FTIR DS, keeping the above discussion in mind, however.

Since the bands in the static FTIR DS are mostly characteristic of P700 or $P700^+$ (*22*), subtracting the static, photoaccumulated FTIR DS from the time-resolved FTIR DS, in a manner that minimizes the intensity of bands due to P700 and $P700^+$ in the resultant spectrum, should account for differences in populations of $P700^+$ that may arise in the two different measurements. If not, then the many diagnostic bands of P700 and $P700^+$ would also show up in the subtracted spectrum. This is found not to be the case in our spectra, so our normalization procedure well accounts for differences in populations of P700 and $P700^+$ in the two spectra.

Since we have subtracted a static FTIR DS from a time-resolved FTIR DS, it is implicitly assumed that the $P700^+$ species that contributes to each spectrum has identical vibrational structure. That is, the $P700^+$ species that contributes to the static FTIR DS does not represent some relaxed species that is somehow different from the transient species. Previously, we have demonstrated that time-resolved and static $P700^+/P700$ FTIR DS are quite similar (*13*). Others have also demonstrated that time-resolved and static $P700^+/P700$ visible DS are similar (*13*, *18*, *25*). In addition, $P^+Q_A^-/PQ_A$ FTIR DS were found to be the same within the noise when collected by time-resolved or photoaccumulation techniques (*26*, *27*). These previous works, as well as the data presented here, then suggest that it is appropriate to subtract static FTIR DS from TR FTIR DS, and in so doing an A_1^-/A_1 FTIR DS will be produced that contains minimal contributions from bands associated with P700 or $P700^+$. This possibility is considered further, with different sets of spectra, in Supporting Information.

Removal of F_X in PS I Considerably Impacts the A_1 Binding Site. Previously we have obtained photoaccumulated A_1^-/A_1 FTIR DS at RT for PS I particles from *S. 6803* that have been stripped of all of the iron sulfur clusters (*23*). These complexes that lack the iron sulfur clusters were obtained by incubating isolated PS I particles in very high concentrations of urea. The A_1^-/A_1 FTIR DS presented here (Figures 4 and 5) are very different from the spectra obtained previously. Hence we believe that the harsh preparation procedure used previously led to considerable modification of the A_1 binding site. These modifications introduced bands into the spectra that are extremely difficult to interpret. In the present paper we have used only intact PS I particles, and so we avoid any ambiguity that could arise because of preparation-induced modification of the A_1 binding site. Recently we have also obtained photoaccumulated FTIR DS for *rubA* mutant PS I particles. These PS I particles also lack all of the iron sulfur clusters (*16*, *28*). The FTIR DS we obtained for the *rubA* mutant PS I particles are also very different from the spectra presented here (data not shown) and again we conclude that removal of F_X considerably impacts the A_1 binding site, introducing bands into the spectra that cannot be easily interpreted. The nature of the introduced bands could be investigated by FTIR DS in combination with isotope-labeled PS I particles. However, it is more appropriate to first characterize the A_1 binding site in intact PS I particles.

Comparison of FTIR DS Obtained from Monomeric and Trimeric PS I. A_1^-/A_1 FTIR DS obtained for trimeric PS I particles from *S. 6803* and *S. 7002* are very similar (spectra b and c in Figure 5). The spectra obtained for monomeric and trimeric PS I particles appear to differ in several spectral regions, however (spectra c and d in Figure 5). Below it will become clear that both sets of spectra can be interpreted similarly, with the only exception being that some of the band frequencies (and intensities) are slightly modified.

13^3 Ester C═O Mode of A_0 Contributes to A_1^-/A_1 FTIR DS. In the *S. 7002* $^1H/^2H$ A_1^-/A_1 FTIR DS, a difference band is observed at 1754(+)/1749(−)/1749(+)/1741(−) cm^{-1}, respectively. A similar difference band is observed at 1754(+)/ 1749(−) cm^{-1} in ^1H and ^{15}N *S. 6803* A_1^-/A_1 FTIR DS and at 1711(+)/1704(−) cm^{-1} in the ^{13}C *S. 6803* A_1^-/A_1 FTIR DS (Figure 5A). As shown in Figure 3, the 1754(+) and 1749(−) cm^{-1} difference bands, as well as their decay, are well resolved.

The 1754(+)/1749(−) cm^{-1} difference band downshifts 5−8 cm^{-1} upon deuteration, ~0 cm^{-1} upon ^{15}N labeling, and 43−45 cm^{-1} upon ^{13}C labeling (Figure 5A). The frequency and the isotope-induced downshifts are consistent with the 1754(+)/1749(−) cm^{-1} difference band being due to a 13^3 ester C═O mode of a chlorophyll-*a* species (*19*, *29*).

It is unlikely that the ~1754(+)/1749(−) cm^{-1} difference band in the unlabeled A_1^-/A_1 FTIR DS is due to an amide I mode because then the band would be expected to downshift ~38 cm^{-1} upon ^{13}C labeling (Figure 6), rather

than the observed 44 cm^{-1}. In addition, it is unlikely that an amide I mode would have such a high frequency.

The 1754(+)/1749(−) cm^{-1} difference band in the ^1H A_l^-/A_l FTIR DS is also unlikely to be due to a protonated carboxylic acid residue. Carboxylic acid C═Os are known to absorb in the 1770−1720 cm^{-1} region (*30*). GluA702 and GluA699 are near A_{1-A} (Figure 1D) and could be impacted by the electrostatic field generated upon A_1 reduction. In fact, mutation of the corresponding residues in *C. reinhardtii* (GluA695 and GluA698) to Gln leads to an ∼55−93% increase in the time constant governing forward ET from A_1^- to F_X (*5*). One argument against this proposal, however, is that carboxylic acid C═O modes are known to downshift >10 cm^{-1} upon deuteration (*31, 32*). This is not observed, so the 1755(+)/1749(−) cm^{-1} difference band in the ^1H A_l^-/A_l FTIR DS is not due to a protonated carboxylic acid residue.

The 1754(+)/1749(−) cm^{-1} difference band is not due to a carboxylic acid C═O mode, and its frequency is higher than would be expected for any other amino acid mode. So the 1754(+)/1749(−) cm^{-1} difference band is not due to a protein mode. In particular, it cannot be due to a protein mode that is impacted by F_X reduction.

Since the 13^3 ester C═O mode of P_B gives rise to the 1754(+)/1749(−) cm^{-1} difference band in static $P700^+/P700$ FTIR DS (*19*, *29*), one possibility is that the 1754(+)/1749(−) cm^{-1} difference band in the ^1H A_l^-/A_l FTIR DS is due to the 13^3 ester C═O mode of P_B that shows up because there is a difference in concentration of $P700^+$ in the static and time-resolved experiments. This hypothesis is unlikely, however. If a difference band due to the 13^3 ester C═O mode of $P700^+/P700$ appears in the A_1^-/A_1 FTIR DS, then many of the other bands of $P700^+/P700$ should also show up in the A_1^-/A_1 FTIR DS. This is not observed.

The fact that a complete difference band at 1754(+)/1748(−) cm^{-1} band is observed in the A_l^-/A_l FTIR DS, and not just a positive band at 1754(+) cm^{-1}, also suggests that the 1754(+)/1748(−) cm^{-1} band cannot be due to the 13^3 ester C═O mode of P_B that somehow arises because the static and time-resolved spectra of P700 are different. This statement is based on the fact that the ground state is the same in both the static and time-resolved experiments, so only differences in $P700^+$ in the static and time-resolved spectra could contribute to the A_l^-/A_l FTIR DS. Because of this it is unlikely that a complete difference band associated with P700 would show up in the A_l^-/A_l FTIR DS.

The most likely possibility is that the 1754(+)/1749(−) cm^{-1} difference band is due to the 13^3 ester C═O mode of A_0 [probably A_{0-A} (*6*, *7*)] that is impacted by the presence of a negative charge on A_1. Several lines of evidence support this hypothesis: (1) Figure 1C indicates that A_{1-A} is coupled to A_{0-A} through the protein. The 13^3 ester C═O of A_{0-A} is 8.28 Å from the closest carbonyl oxygen of A_{1-A} and 3.47 Å from TrpA697 (Figure 1B). (2) The 1754(+)/1749(−) cm^{-1} band displays ^2H, ^{15}N, and ^{13}C isotope-induced downshifts that are typical for 13^3 ester C═O modes of chlorophyll *a*. (3) In FTIR DS studies of PBRCs from *Rhodopseudomonas viridis* (*33*−*35*) and *Rb. sphaeroides* (*35*, *36*) it has been established that the 13^3 ester C═O of H_A (the electron-accepting bacteriopheophytin) is impacted by the electrostatic field generated upon Q_A^- formation, as a difference band associated with the H_A 13^3 ester C═O is clearly present in Q_A^-/Q_A FTIR DS. In PBRCs, Q_A is greater than 10 Å from H_A. This distance is considerably larger than the distance between the 13^3 ester carbonyl oxygen of A_{0-A} and the closest carbonyl oxygen of A_{1-A} (Figure 1). The data from Q_A^-/Q_A FTIR DS then suggest that it is likely that that there will be a long-range electrostatic interaction between A_0 and A_1^- in PS I.

Further evidence supporting long-range electrostatic effects in PS I is the observation that a carotenoid absorption band is shifted upon A_1 reduction (*37*). This electrochromic band shift is most clearly observed at ∼480 nm in time-resolved pump−probe measurements (*8*). The carbonyl oxygens of A_{1-A} are between 7 and 9 Å from the ring atoms of the closest β-carotene [labeled BCR4014 on the PsaA side in the PS I crystal structure (1JB0)].

Recently, we have obtained A_l^-/A_l FTIR DS for PS I particles in which the methionine axial ligands of A_{0-A}/A_{0-B} (MetA688 and MetB668) are changed to leucine (*38*). In these spectra the 1754(+)/1749(−) cm^{-1} difference band is not observed when MetA688 is changed but is unaffected when MetB668 is changed (*38*). These observations provide further support for the hypothesis that the 1754(+)/1749(−) cm^{-1} difference band in A_l^-/A_l FTIR DS is due to the 13^3 ester C═O of A_{0-A}.

We note that the 13^3 ester C═O mode of H_A, observed at 1736(−) cm^{-1} in Q_A^-/Q_A FTIR DS from *Rps. viridis*, downshifts ∼6 cm^{-1} upon Q_A reduction (*33*). In contrast, the 1754(+)/1749(−) cm^{-1} band observed in ^1H A_l^-/A_l FTIR DS indicates a 5 cm^{-1} upshift. It is not clear if the electrochromic response of the 13^3 ester C═O mode of A_0 to A_1 reduction should lead to a downshift or upshift. The direction of the shift will depend on the geometry of the C═O bond relative to the geometry of the negative charge on A_{1-A}. This idea is highlighted by the observation that the 13^1 keto C═O mode of H_A, observed at 1676(−) cm^{-1} in Q_A^-/Q_A FTIR DS from *Rps. viridis*, upshifts ∼9 cm^{-1} upon Q_A reduction (*33*).

If the electronic structure of A_0 is perturbed by A_1 reduction, it would be reasonable to assume that A_1 is impacted by A_0 reduction. It is unclear if this type of electrostatic effect could modify the electronic structure of A_1 in a way that could contribute to the extreme rapidity of secondary electron transfer in PS I [∼21 ps (*25*)]. One argument against such a proposal is that a similar type of electrostatic effect is observed in PBRCs, and secondary ET proceeds much more slowly (∼200 ps). However, this slower rate could also be partially related to the fact that the distance between the bacteriopheophytin and Q_A cofactors in PBRCs is larger than the distance between A_0 and A_1 in PS I (see above).

Figure 1B indicates that there is a coupling between the A_{0-A} and A_{1-A} pigments, involving TrpA697, TyrA696, and MetA688. Such a structural arrangement, between Q_A and BPheo, does not exist in purple bacteria, and it might therefore be possible that this structural arrangement could contribute to the extreme reduction potential that is associated with A_1 in PS I. This idea might be testable by studying mutant cyanobacterial PS I particles in which TyrA696 has been changed.

Does the 13^1 Keto C═O Mode of A_0 Contribute to A_1^-/A_1 FTIR DS? If a 13^3 ester C═O mode of A_0 contributes to A_l^-/A_l FTIR DS, it is reasonable to suggest that the 13^1 keto

Table 1: Band Frequencies for Labeled and Unlabeled PS I Particles from *S. 6803* and *S. 7002* with Proposed Band Assignments[a]

strain (label)	1	2	3	4	5	6	7	8	9	10	11	12	13
S. 6803$_M$	1754(+)	1749(−)	1693(−)	1674(+)	1666(−)	1656(−)	1648(−)	1634(−)[b]	1607(−)	1558(−)	1546(−)	1495(+)	1414(+)[c]
S. 6803$_T$	1754(+)	1749(−)	1693(−)	1677(+)	1666(−)	1655(−)	1651(−)	1634(−)[b]	1607(−)	1558(−)	1546(−)	1495(+)	1414(+)[c]
S. 6803$_M$ (^{13}C)	1711(+)	1704(−)	1647(−)	1636(+)	1623(−)	1611(−)	1597(−)	1579(−)	1563(−)	1536(−)	1528(−)	1454(+)	1355(+)
S. 6803$_M$ (^{15}N)	1754(+)	1748(−)	1693(−)	1675(+)	?	?	?	1634(−)	1607(−)	1546(−)	1534(−)	1495(+)	1414(+)
S. 7002$_T$	1754(+)	1749(−)	1695(−)	1677(+)	1666(−)	1655(−)	1652(−)	1634(−)	1607(−)	1558(−)	1549(−)	1495(+)	1414(+)
S. 7002$_T$ (^{2}H)	1749(+)	1741(−)	1691(−)	1669(+)	1658(−)[d]	1652(−)	1652(−)	1621(−)	1601(−)	1473(−)	1463(−)	1483(+)	1412(+)

[a] Proposed band assignments: (1) 13^3 ester C═O of A_0 in the A_1^- state; (2) 13^3 ester C═O of A_0 for neutral A_1; (3) 13^1 keto C═O of A_0 for neutral A_1; (4) amide I mode; (5) amide I mode; (6) C═O mode of neutral A_1, free from H-bonding; (7) C═C mode of neutral A_1; (8) C═C mode for neutral A_1; (9) C═O mode of A_1 that is H-bonded; (10) amide II mode; (11) amide II mode; (12) C⋯O mode of A_1^-; (13) C⋯C mode of A_1^-. [b] Partly due to an amide I mode also. [c] Tentative. [d] Shoulder.

C═O mode of A_0 should also contribute. Figure 1B indicates that the 13^1 keto carbonyl oxygen of A_{0-A} could be H-bonded to TyrA696. The hydroxyl oxygen of TyrA696 is 8.97 Å from the closest carbonyl oxygen of A_{1-A} (not shown). If the 13^1 keto C═O of A_{0-A} is weakly H-bonded, then this mode might absorb in the ∼1700−1670 cm^{-1} region. If the H-bond is stronger, then the C═O mode might be expected to show up in the ∼1670−1640 cm^{-1} region. In FTIR DS studies of PBRCs from *Rps. viridis* (*33*−*35*) and *Rb. sphaeroides* (*35*, *36*), it has been established that the 13^1 keto C═O of H_A is impacted upon Q_A^- formation: in *Rps. viridis* the 13^1 keto C═O of H_A is H-bonded to GluL104 and absorbs at 1676 cm^{-1}. Upon Q_A^- formation this band upshifts 9 cm^{-1}.

In the ^{1}H *S. 7002* A_l^-/A_l FTIR DS, a difference band is observed at 1709(+)/1695(−) cm^{-1} and appears to downshift 4/4 cm^{-1} to 1705(+)/1691(−) cm^{-1} upon deuteration. The 1691(−) cm^{-1} band in the ^{2}H A_l^-/A_l FTIR DS is obscured by a positive feature at 1685 cm^{-1} that is not present in the ^{1}H spectrum. In ^{1}H and ^{15}N *S. 6803* A_l^-/A_l FTIR DS, a negative band is observed at 1693 cm^{-1}, but no clear positive band is observed near 1709 cm^{-1}. It is likely that the 1693(−) cm^{-1} band in the ^{1}H *S. 6803* A_l^-/A_l FTIR DS downshifts 46 cm^{-1} to 1647 cm^{-1} upon ^{13}C labeling (Figure 5A).

A frequency of 1693−1695 cm^{-1}, as well as ^{2}H/^{15}N/^{13}C isotope-induced shifts of 4/0/46 cm^{-1}, respectively, all point to the suggestion that this band is due to a 13^1 keto C═O mode of a chlorophyll *a* species, most likely the 13^1 keto C═O mode of A_{0-A}.

In the *S. 7002* A_1^-/A_1 FTIR DS a positive band is observed at 1709(+) cm^{-1}, which leads to the suggestion that the 1695(−) cm^{-1} band upshifts 14 cm^{-1} upon A_1^- formation. However, the ^{15}N- and ^{13}C-labeled spectra in Figure 5A appear to be more consistent with an upshift of 8 and 10 cm^{-1} upon A_1^- formation, respectively. Irrespective of the precise anion-induced frequency shift of the 1693−1695 cm^{-1} band in A_1^-/A_1 FTIR DS, we assign it to a 13^1 keto C═O mode of A_0 and tentatively suggest that it upshifts upon anion formation. One point of note is that the 13^1 keto C═O group of A_{0-A} could be H-bonded to TyrA696 and that the tyrosine hydroxyl side chain could also be impacted upon deuteration. So it is not entirely clear precisely what should happen to the 13^1 keto C═O mode of A_{0-A} upon deuteration. Finally, a frequency of 1693−1695 cm^{-1} for a 13^1 keto C═O mode of A_{0-A} suggests that it can only be very weakly H-bonded to TyrA696.

If the H-bond to the 13^1 keto C═O of A_0 is not so weak, then it may absorb in the 1670−1640 cm^{-1} region. In the A_l^-/A_l FTIR DS, many difference bands appear to contribute in this region (see below); thus definitive assignment of bands to 13^1 keto C═O modes of A_0 is difficult. Ambiguity in assigning bands to the 13^1 keto C═O mode of A_0 could possibly be removed by producing A_l^-/A_l FTIR DS for PS I particles in which TyrA696 has been mutated to a non-H-bonding residue.

Amide II Absorption Bands in A_1^-/A_1 FTIR DS. Intense negative difference bands are observed at 1549 and 1559 cm^{-1} in the ^{1}H *S. 7002* A_1^-/A_1 FTIR DS (Figure 5B). Each of these negative difference features appears to downshift 86 cm^{-1} to 1463/1473 cm^{-1} upon deuteration (Figure 5B). In both trimeric and monomeric ^{1}H *S. 6803* A_1^-/A_1 FTIR DS, two bands are observed at 1559(−) and 1546(−) cm^{-1}. These bands likely correspond to the 1549(−) cm^{-1} and 1559(−) cm^{-1} bands observed in the ^{1}H *S. 7002* A_1^-/A_1 FTIR DS. Upon ^{15}N labeling, a negative band is found at 1534 cm^{-1}, with shoulders at 1540 and 1546 cm^{-1} (Figure 5B). It is likely that the 1559(−) and 1546(−) cm^{-1} bands in the ^{1}H *S. 6803* A_1^-/A_1 FTIR DS downshift 13 and 12 cm^{-1}, respectively, to 1546(−) and 1534(−) cm^{-1} upon ^{15}N labeling. Upon ^{13}C labeling, an intense negative band is observed at 1536 cm^{-1}, with a shoulder at 1527 cm^{-1}. Upon ^{13}C labeling, one interpretation could be that the 1559(−) and 1546(−) cm^{-1} bands in the ^{1}H *S. 6803* A_1^-/A_1 FTIR DS downshift 23 and 19 cm^{-1}, respectively. Although a ^{13}C-induced downshift 19−23 cm^{-1} for an amide II mode is greater than the ∼13 cm^{-1} shift that would be predicted on the basis of the IR absorption spectra (Figure 6), it might still be reasonable. Therefore, the frequency of the two bands [1559(−) and 1549−1546(−) cm^{-1}], as well as all of the isotope labeling data, are consistent with the assignment of these bands to amide II modes (see Table 1).

In summary, two bands appear in the 1560−1540 cm^{-1} region in both the unlabeled *S. 6803* and *S. 7002* A_1^-/A_1 FTIR DS. The two bands downshift ∼86/12 cm^{-1} upon ^{2}H/^{15}N labeling, respectively. Amide II absorption bands are known to downshift ∼14 cm^{-1} upon ^{15}N labeling and ∼100 cm^{-1} upon deuteration (Figure 6), so it is natural to assign the two bands at 1559(−) and 1549−1546(−) cm^{-1} in the ^{1}H *S. 7002* and *S. 6803* A_1^-/A_1 FTIR DS to amide II modes.

Amide I Absorption Bands. Since amide II absorption bands contribute to A_1^-/A_1 FTIR DS, amide I absorption bands should also contribute. Amide I absorption bands generally occur in the 1680−1630 cm^{-1} spectral region (Figure 6). The most obvious candidate for an amide I absorption band in the ^{1}H trimeric *S. 6803* and *S. 7002* A_1^-/A_1 FTIR DS is the 1677(+)/1666(−) cm^{-1} difference band (spectra c and b, Figure 5A). The positive band at 1674(+) cm^{-1} in monomeric ^{1}H *S. 6803* A_1^-/A_1 FTIR DS probably

corresponds to the 1677(+) cm^{-1} band in the trimeric ^1H A_1^-/A_1 FTIR DS (see below).

Excited-State Amide I Absorption Bands. Upon ^2H labeling, the 1677(+) cm^{-1} difference band in the unlabeled *S. 7002* A_1^-/A_1 FTIR DS downshifts 8 cm^{-1} to 1669(+) cm^{-1}. Although the spectra in Figure 6 indicate that amide I bands downshift ~12 cm^{-1} upon deuteration at RT, a downshift of 8 cm^{-1} upon deuteration at 77 K is not unreasonable. Therefore, the unlabeled and deuterated data support the suggestion that the 1677(+) cm^{-1} band in the trimeric ^1H A_1^-/A_1 FTIR DS is due to an amide I mode. The 1674(+) cm^{-1} band in the monomeric ^1H *S. 6803* A_1^-/A_1 FTIR DS appears to downshift 38 cm^{-1}, to 1636 cm^{-1}, upon ^{13}C labeling and is little impacted upon ^{15}N labeling (Figure 5A). A 38 cm^{-1} ^{13}C-induced shift and only a small shift upon ^{15}N labeling are as expected for an amide I mode (Figure 6). Therefore, we assign the 1674(+) cm^{-1} band in monomeric ^1H *S. 6803* A_1^-/A_1 FTIR DS to an amide I mode (Table 1).

Ground-State Amide I Absorption Bands. Above it was suggested that the negative band at 1666(−) cm^{-1} in the unlabeled *S. 7002* A_1^-/A_1 FTIR DS could be due to an amide I mode. Upon deuteration of PS I from *S. 7002*, a negative band is observed at 1652(−) cm^{-1} with a shoulder at 1658(−) cm^{-1} (Figure 5A). These data suggest that the 1666(−) cm^{-1} band could downshift 14 or 8 cm^{-1} to 1652(−) or 1658(−) cm^{-1} upon deuteration, respectively. Below we suggest that the 1652(−) cm^{-1} band in the ^2H A_1^-/A_1 FTIR DS is not due to amide I. Given this, we then associate the 1658(−) cm^{-1} shoulder in the ^2H A_1^-/A_1 FTIR DS with an amide I mode. That is, the 1666(−) cm^{-1} band in the ^1H A_1^-/A_1 FTIR DS downshifts 8 cm^{-1} upon deuteration (Table 1).

Although a band at 1666(−) cm^{-1} in trimeric ^1H A_1^-/A_1 FTIR DS is assigned to an amide I mode, a corresponding band in monomeric ^1H *S. 6803* A_1^-/A_1 FTIR DS is not so obvious. In the monomeric ^1H *S. 6803* A_1^-/A_1 FTIR DS, three negative features are observed at 1666, 1656, and 1648 cm^{-1}. In the ^{13}C *S. 6803* A_1^-/A_1 FTIR DS, three negative features are also observed at 1623, 1611, and 1597 cm^{-1} (Figure 5A).

The 1656 cm^{-1} feature in the ^1H *S. 6803* A_1^-/A_1 FTIR DS could downshift 33, 45, or 59 cm^{-1} to 1623, 1611, or 1597 cm^{-1}, respectively, upon ^{13}C labeling. Thus the 1656 cm^{-1} feature could be due to an amide mode, a C═O mode, or a C═C mode of A_1, respectively. An amide I mode is expected to downshift more than 33 cm^{-1} upon ^{13}C labeling, while a C═C mode is expected to shift less than 59 cm^{-1} upon ^{13}C labeling. The 1656 cm^{-1} feature is therefore likely due to a C═O mode of neutral A_1.

The 1666 cm^{-1} feature in the ^1H *S. 6803* A_1^-/A_1 FTIR DS could downshift 43 or 55 cm^{-1} to 1623 or 1611 cm^{-1} upon ^{13}C labeling. Thus the 1666 cm^{-1} feature could be due to a C═O or C═C mode of A_1, respectively. It could also be associated with an amide I mode, although a ^{13}C-induced downshift of ~43 cm^{-1} is rather high.

The 1648 cm^{-1} feature in the ^1H *S. 6803* A_1^-/A_1 FTIR DS could downshift 37 or 51 cm^{-1} to 1611 or 1597 cm^{-1} upon ^{13}C labeling. Thus the 1648 cm^{-1} feature could be due to an amide I mode or a C═C mode of A_1, respectively. It is unlikely that 1648 cm^{-1} feature is due to a C═O mode of A_1, as a downshift of ~44 cm^{-1} would be expected.

If the three negative features at 1666, 1656, and 1648 cm^{-1} in the monomeric ^1H *S. 6803* A_1^-/A_1 FTIR DS correspond to the three bands at 1623, 1611, and 1597 cm^{-1} in the ^{13}C *S. 6803* A_1^-/A_1 FTIR DS and the three bands correspond to three different modes (an amide I mode, a C═O mode, and a C═C mode of A_1), then it is logically the case that the 1656 cm^{-1} band cannot be due to an amide I mode. The most likely scenario is that the 1666 cm^{-1} feature in the monomeric ^1H *S. 6803* A_1^-/A_1 FTIR DS is due to an amide I mode (the actual mode frequency is probably less than 1666 cm^{-1}). The 1656 cm^{-1} band is then due to a C═O mode and the 1648 cm^{-1} band is due to a C═C mode. This set of assignments is consistent with the following two observations: (1) It is well-known from experiment (*24*) and calculation (*39*, *40*) that quinone C═O modes absorb at higher frequencies than quinone C═C modes. (2) PhQ C═O modes in vivo absorb at lower frequency than in vitro (*24*). The PhQ C═O mode absorbs at 1661 cm^{-1} in vitro. Therefore, the 1666(−) cm^{-1} feature in the ^1H *S. 6803* A_1^-/A_1 FTIR DS cannot be due to a C═O mode (or a C═C mode) of A_1. It is therefore most likely due to an amide I mode.

In summary, the 1666(−) cm^{-1} features in both monomeric and trimeric ^1H A_1^-/A_1 FTIR DS have the same origin (Table 1). The 1656(−)/1648(−) cm^{-1} bands in the monomeric ^1H *S. 6803* A_1^-/A_1 FTIR DS downshift 45/51 cm^{-1} to 1611/1597 cm^{-1} upon ^{13}C labeling and are due to C═O/C═C modes of A_1, respectively.

Difficulty in assigning bands in the 1666−1648(−) cm^{-1} region in the ^1H *S. 6803* A_1^-/A_1 FTIR DS is compounded partly because the changes in the ^{15}N A_1^-/A_1 FTIR DS, in the 1670−1640 cm^{-1} region, are complex: Upon ^{15}N labeling, the 1656(−) cm^{-1} band in the ^1H *S. 6803* A_1^-/A_1 FTIR DS is considerably altered, with a complicated set of features appearing at 1657(+)/1653(+)/1644(−) cm^{-1} (Figure 5A). These features may suggest the appearance of a new band at ~1654(−)/1667(+) cm^{-1} upon ^{15}N labeling. The complexity of the ^{15}N-induced changes in the spectra may not be surprising since several molecular modes will be impacted by ^{15}N labeling. First, amide I modes are affected upon ^{15}N labeling, downshifting 1−2 cm^{-1}. Second, side-chain modes of tryptophan residues will also be impacted upon ^{15}N labeling. Since Trp residues are close to A_1 in PS I (Figure 1A), it could be possible that ^{15}N changes in Trp residues contribute to the complexity of the ^{15}N A_1^-/A_1 FTIR DS. For Trp in solution, it is found that Trp NH modes appear at ~1622 cm^{-1} (*41*). So a frequency of 1656 cm^{-1} appears too high for a Trp NH mode. Finally, above it was suggested that modes of A_1 are found in the 1656−1648 cm^{-1} region. If the ^{15}N label impacts the nearby indole nitrogen of Trp, then it is possible that the C═O modes of A_1 will also be modified upon ^{15}N labeling. Therefore, complex changes in the A_1^-/A_1 FTIR DS in the ~1660−1640 cm^{-1} region appear to be quite likely upon ^{15}N labeling. Although we are unable to clearly resolve the spectral details, the complexity of the changes observed upon ^{15}N labeling is a likely indication that the π-stacked Trp residue has a considerable impact on the electronic structure of A_1.

C═O and C═C Modes of A_1. In A_1^-/A_1 FTIR DS, negative bands associated with C═O and C═C modes of A_1 are expected to appear in the 1700−1600 cm^{-1} spectral region. Possible bands in the trimeric ^1H A_1^-/A_1 FTIR DS

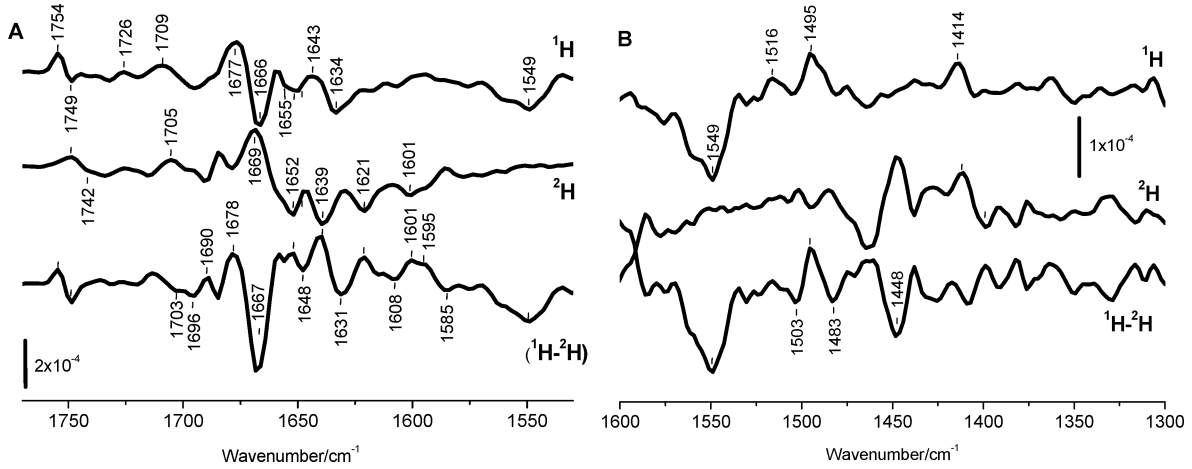

FIGURE 7: (A, B) A_1^-/A_1 FTIR DS obtained for unlabeled (^{1}H) (top) and deuterated (^{2}H) (middle) PS I particles from *S. 7002*. The (^{1}H−^{2}H) FTIR double difference spectrum (DDS) is also shown (bottom). The ^{1}H and ^{2}H spectra were first normalized so that the 1677(+)/1666(−) (^{1}H spectrum) and 1669(+)/1652(−) cm^{-1} (^{2}H spectra) bands were similar in intensity.

that could be associated with C═O and C═C modes of A_1 are observed at 1655, 1651, 1634, 1628 (shoulder), and 1607 cm^{-1} (spectra b and c, Figure 5A). Above we suggested that bands at 1655 and 1651−1648 cm^{-1} are due to C═O and C═C modes of A_1, respectively,

Is the Negative Band at 1634 cm^{-1} Due to a C═C Mode of A_1? A negative band appears at 1634(−) cm^{-1} in all ^{1}H A_1^-/A_1 FTIR DS (Figure 5A). The 1634 cm^{-1} band is unaffected by ^{15}N labeling. Upon ^{13}C labeling, the 1634 cm^{-1} band could downshift 37 or 55 cm^{-1} to 1597 or 1579 cm^{-1}. If the 1634 cm^{-1} band downshifts 55 or 37 cm^{-1} upon ^{13}C labeling, then it is likely due to a C═C mode of A_1 or an amide I mode, respectively. Therefore, the ^{13}C isotope labeling data cannot clearly distinguish if the 1634 cm^{-1} band is due to a quinone C═C or an amide I mode. Above we suggested that the 1648 cm^{-1} band in ^{1}H *S. 6803* A_1^-/A_1 FTIR DS could downshift to 1597 cm^{-1} upon ^{13}C labeling. If this is correct then the 1634 cm^{-1} band in ^{1}H *S. 6803* A_1^-/A_1 FTIR DS downshifts 55 cm^{-1} upon ^{13}C labeling and is therefore due to a quinone C═C mode (see Table 1).

Upon ^{2}H labeling, it appears to be the case that the 1634 cm^{-1} band in ^{1}H *S. 7002* A_1^-/A_1 FTIR DS downshifts 13 cm^{-1} to 1621 cm^{-1} (Figure 5A). A 13 cm^{-1} ^{2}H-induced downshift could be expected for an amide I mode (Figure 6). From recent density functional calculations of gas-phase naphthoquinone (NQ) derivatives, we have found that aromatic and quinone ring C═C modes downshift ∼10 and 30 cm^{-1}, respectively, upon ^{2}H labeling (data not shown). In addition, C═O modes are little affected by deuteration. On the basis of these calculations, one could favor the hypothesis that the 1634 cm^{-1} band is due to a C═C mode, and not a C═O mode, of neutral A_1.

Due to spectral overlap of several bands, it is difficult to unambiguously characterize deuterium-induced difference band shifts simply by comparing the ^{1}H and ^{2}H A_1^-/A_1 FTIR DS. To try to gain a more detailed characterization of the deuterium-induced band shifts, we have calculated a (^{1}H−^{2}H) A_1^-/A_1 FTIR DS, which is shown in Figure 7. The second derivative feature at 1639(+)/1631(−)/1621(+) cm^{-1} in the (^{1}H−^{2}H) A_1^-/A_1 FTIR DS suggests that a difference band at ∼1639(+)/1631(−) cm^{-1} in the ^{1}H A_1^-/A_1 FTIR DS downshifts ∼8/10 cm^{-1} to ∼1631(+)/1621(−) cm^{-1} in the ^{2}H A_1^-/A_1 FTIR DS. This conclusion is not at all obvious from consideration of the ^{1}H and ^{2}H A_1^-/A_1 FTIR DS. A ^{2}H-induced downshift of 8−10 cm^{-1} for the 1639(+)/1631(−) cm^{-1} band suggests that this band is due to an amide I mode. The fact that a complete difference band is observed, and not a single negative band, also suggests the presence of an amide I mode rather than a C═C mode (in the latter case only a single negative feature is expected rather than a difference feature).

In summary we conclude that the difference band at ∼1643(+)/1634(−) cm^{-1} in the ^{1}H A_1^-/A_1 FTIR DS appears to be partly due to an amide I band. In addition, we also conclude that part of the 1634(−) cm^{-1} band appears to be due to a C═C mode of neutral A_1 (see Table 1).

C═O Modes of A_1. To consider the origin of bands in A_1^-/A_1 FTIR DS, it is useful to consider what is known about PhQ modes in vitro and when incorporated into the Q_A site in PBRCs. For PhQ in vitro, a C═O absorption band is observed at ∼1661 cm^{-1} (*23*, *24*, *42*). More specifically, the normal mode giving rise to most of the intensity of the 1661 cm^{-1} band is an asymmetric stretching vibration of both C═O groups. Bands due to quinone and aromatic C═C modes of the NQ ring are found at 1618 and 1597 cm^{-1}, respectively (*24*).

From Q_A^-/Q_A FTIR DS obtained for PBRCs from *Rb. sphaeroides* reconstituted with PhQ, it was suggested that bands associated with the C═O modes are found at 1651 and 1640 cm^{-1}, while bands associated with the C═C modes are found at 1608 and 1588 cm^{-1} (*24*). However, from studies of site-specifically ^{13}C-labeled ubiquinones reconstituted into PBRCs of *Rb. sphaeroides*, it was found that bands at 1660, 1628, and 1601 cm^{-1} in Q_A^-/Q_A FTIR DS are due predominantly to C_1═O, C═C, and C_4═O modes, respectively (*43*). That is, one of the C═O modes absorbs at a lower frequency than one of the C═C modes. Irrespective of the precise assignments, two bands are observed that are associated with C═O modes of the quinone that is reconstituted into the Q_A site. This is expected since the quinone C═Os are differently H-bonded in the Q_A site in PBRCs. For PhQ in PS I, the C═Os are also differentially H-bonded (Figure 1), so one might expect to observe at least two bands associated with A_1 C═O modes. This is especially so since it has been suggested that the H-bond to one of the C═Os of A_1 is very strong (*44*).

Above it was suggested that the negative band near 1655−1651 cm^{-1} in the trimeric ^1H A_1^-/A_1 FTIR DS is due to a PhQ C═O mode. Between 1645 and 1660 cm^{-1} the features in the ($^1H-^2H$) FTIR DDS are very weak, indicating that the features between 1655 and 1651(−) cm^{-1} are little impacted by deuteration. Therefore, the negative feature at 1655−1651 cm^{-1} in the *S. 7002* ^1H A_1^-/A_1 FTIR DS is most likely due to a C═O mode of neutral A_1. We can rule out the possibility that the 1655−1651(−) cm^{-1} feature in the ^1H *S. 7002* A_1^-/A_1 FTIR DS is due to C═C modes of neutral A_1, as a ^2H-induced downshift of >10 cm^{-1} would then be expected (G.H., unpublished calculations). A frequency of 1655−1651 cm^{-1} for a PhQ C═O mode suggests that it is free from H-bonding.

In Q_A^-/Q_A FTIR DS obtained for PBRCs, the H-bonded quinone C═O mode absorbs near 1600 cm^{-1}, suggesting a very strong H-bond. In recent electron paramagnetic resonance (EPR) studies of A_1 in PS I, it was also suggested that a very strong H-bond exists between the PhQ carbonyl and the backbone oxygen of LeuA722 (Figure 1A) (*44*). If this is the case, then we may expect to find bands associated with H-bonded C═O modes of neutral A_1 below ∼1620 cm^{-1}. It is possible that the band at 1607 cm^{-1} in the ^1H *7002* A_1^-/A_1 FTIR DS is due to strongly H-bonded PhQ C═O mode and that it downshifts 6 cm^{-1} to 1601 cm^{-1} upon deuteration. A band is also observed near 1607 cm^{-1} in the ^1H and ^{15}N *S. 6803* A_1^-/A_1 FTIR DS and could downshift 44 cm^{-1} to 1563 cm^{-1} upon ^{13}C labeling. The isotope labeling data are therefore consistent with the 1607 cm^{-1} band being due to an H-bonded quinone C═O mode (see Table 1).

C⋯O and C⋯C Modes of A_1^-. Semiquinone C⋯O and C⋯C modes display positive bands in the ∼1520−1380 cm^{-1} region. In Q_A^-/Q_A FTIR DS obtained for PBRCs from *Rps. viridis* and *Rb. sphaeroides* reconstituted with vitamin K_1 in the Q_A site,[5] three well-separated bands are observed at 1478(+), 1444−1438(+), and 1394−1392(+) cm^{-1} (*24*). These bands were assigned to semiquinone C⋯C, C⋯O, and C⋯C modes, respectively (*24*).

In contrast to the above anion band assignments for vitamin K_1 in the Q_A site in PBRCs, band assignments for quinone anions in vitro appear quite different. Upon electrochemical reduction of a variety of quinones in vitro, quinone C⋯O vibrations were generally found at higher frequency, with greater intensity than bands associated with C⋯C vibrations (*42*).

In both trimeric and monomeric ^1H A_1^-/A_1 FTIR DS, positive bands are observed at ∼1495(+) and 1414(+) cm^{-1} (Figure 5B). Figure 2A shows the time course of the absorption changes at 1495 cm^{-1} following excitation of PS I particles from *S. 7002*. Clearly, the 1495 cm^{-1} band, and its decay, are well resolved.

The A_1^-/A_1 FTIR DS shown here are considerably modified upon ^2H exchange. This is in contrast to Q_A^-/Q_A FTIR DS obtained for PBRCs from *Rps. viridis* and *Rb. sphaeroides* (reconstituted either with vitamin K_1 or with ubiquinone in the Q_A site) that have been ^1H- and ^2H-labeled (*35*), where it is found that deuterium exchange only leads to small modifications in the spectra in the 1500−1400 cm^{-1} region. The 1444−1438(+) cm^{-1} band is the one predominantly affected by ^2H exchange, and this observation led to the suggestion that this band is due to an H-bonded C⋯O mode. However, in the work on PBRCs (*35*), ^2H exchange was achieved via incubation of RCs in D_2O buffer and was estimated to be ∼70%. This is in contrast to the ∼98% ^2H exchange obtained for our PS I particles. In our work all of the hydrogens of PhQ will be exchanged, as will all the hydrogens associated with the amino acids, which may not be the case for the quinones in PBRCs used in previous studies (*35*).

With the use of density functional theory (DFT) to calculate the vibrational mode frequencies of unlabeled and labeled phyllosemiquinone (to be presented elsewhere), we have found that deuteration will induce downshifts of up to 18 cm^{-1}/14 cm^{-1} for C⋯O/C⋯C modes, respectively. This is primarily because the semiquinone C⋯O and C⋯C modes are mixed with C−H bending modes. In addition, from DFT calculations we have found that semiquinone C⋯O/C⋯C modes will be expected to downshift 41 cm^{-1}/57 cm^{-1} upon ^{13}C labeling (not shown).

The 1495(+) cm^{-1} band in the *S. 7002* ^1H A_1^-/A_1 FTIR DS is considerably impacted upon deuteration. The derivative feature at 1495(+)/1483(−) cm^{-1} in the ($^1H-^2H$) A_1^-/A_1 FTIR DDS (Figure 7B) suggests that the 1495 cm^{-1} band downshifts ∼12 cm^{-1} to ∼1483 cm^{-1} upon deuteration. From this ^2H-induced band shift it is difficult to distinguish whether the 1495(+) cm^{-1} band is due to a C⋯O or C⋯C mode.

The 1495 cm^{-1} band in the ^1H *S.6803* A_1^-/A_1 FTIR DS could downshift 41 or 52 cm^{-1} to 1454 or 1443 cm^{-1} upon ^{13}C labeling. So it is still difficult to distinguish unambiguously if the 1495 cm^{-1} band in the unlabeled spectrum is due to a C⋯O or C⋯C mode. However, it has to be the case that at least part of the 1495 cm^{-1} band downshifts to 1454 cm^{-1} upon ^{13}C labeling. Such a downshift is consistent with that part of the 1495 cm^{-1} band being due to a semiquinone C⋯O mode (see Table 1).

From our DFT calculations for PhQ (not shown) and from electrochemically generated semiquinone FTIR DS in vitro (*42*), it has been found that bands associated with semiquinone C⋯O modes are considerably more intense than bands associated with semiquinone C⋯C modes. From this perspective it could be suggested that the 1495 cm^{-1} band in unlabeled spectra is due to a semiquinone C⋯O mode, as it is more intense than other bands in the 1520−1430 cm^{-1} spectral region. However, it should be noted that the band associated with the semiquinone C⋯O mode in Q_A^-/Q_A FTIR DS (obtained for PBRCs with PhQ reconstituted into the Q_A site) is less intense than bands associated with semiquinone C⋯C modes (*24*).

Upon ^{15}N labeling, it appears that a portion of the 1495(+) cm^{-1} band is impacted. However, a narrower band still appears at 1495(+) cm^{-1} in the ^{15}N-labeled A_1^-/A_1 FTIR DS. So some part of the 1495(+) cm^{-1} band in the unlabeled A_1^-/A_1 FTIR DS is affected by ^{15}N labeling. So it appears that the electronic structure of the C⋯O mode of A_1^- is perturbed upon ^{15}N labeling. The only group near A_1 that is impacted by ^{15}N labeling is the indole side chain of Trp. So again, the ^{15}N-labeled spectra suggests some coupling between Trp and PhQ.

[5] Q_A is menaquinone 9 in *Rps. viridis* and ubiquinone 9 in *Rb. sphaeroides*. Menaquinone 9 has the same naphthoquinone headgroup as vitamin K_1 (PhQ).

Finally, we have recently obtained A_1^-/A_1 FTIR DS for *menG* PS I mutants. In the *menG* mutant a PhQ analogue lacking the 2-methyl group is incorporated into the A_1 site in PS I. We have found that the 1495 cm^{-1} band upshifts ~4 cm^{-1} in the *menG* mutant PS I particles (*38*). We have also used DFT to calculate the vibrational properties of the anionic forms of PhQ and its demethylated analogue (*38*), and we calculate that the PhQ anion C⋯O mode upshifts upon demethylation (*38*). Thus our calculations reproduce the experimentally observed trends and support the hypothesis that the 1495 cm^{-1} band is due to a PhQ C⋯O mode.

In the ~1480−1440 cm^{-1} region, deuteration-induced shifts are difficult to analyze, due to interference caused by the appearance of amide II′ absorption bands in the ^2H A_1^-/A_1 FTIR DS. At lower frequency, a positive band is observed at 1414 cm^{-1} in ^1H A_1^-/A_1 FTIR DS. This band is little affected by ^{15}N labeling and downshifts ~2 cm^{-1} upon deuteration (Figure 7B). Our DFT calculations and the observed small deuterium-induced downshift suggest that the 1414 cm^{-1} band is not due to a C⋯O or a C⋯C mode. We note, however, that in Q_A^-/Q_A FTIR DS obtained for PBRCs, a band at 1394(+) cm^{-1} was assigned to a semiquinone C⋯C mode partly on the basis of its insensitivity to deuterium exchange.

Finally, upon ^{13}C labeling, it appears that the 1414(+) cm^{-1} band downshifts ~58 cm^{-1} to 1355(+) cm^{-1} (Figure 5B). Such a shift is consistent with the idea that the 1414(+) cm^{-1} band is due to a semiquinone C⋯C mode. For comparison, in Q_A^-/Q_A FTIR DS obtained for PBRCs from *Rb. sphaeroides* reconstituted with Q_8, a band at 1466(+) cm^{-1} in unlabeled Q_A^-/Q_A FTIR DS was found to downshift 59 cm^{-1}, to 1407 cm^{-1}, upon uniform ^{13}C labeling of Q_8. This observed shift led to the assignment of the 1466(+) cm^{-1} band to a semiquinone C⋯C mode.

Since our data are not entirely conclusive, we only tentatively assign the 1414(+) cm^{-1} band to a C⋯C mode of A_1^- (see Table 1).

CONCLUSIONS

In this paper we present the first A_l^-/A_l FTIR DS that have been obtained for intact PS I particles. Using a variety of isotopically labeled PS I particles, we have also shown that we can start to investigate the origin of bands in the A_l^-/A_l FTIR DS.

We have outlined several possible band assignments (see Table 1). To further test/verify some of these assignments, specific types of labeling strategies and site-directed mutagenesis will be required, and such work is beginning in our lab.

Several bands in the A_l^-/A_l FTIR DS have been assigned: (1) A set of negative difference bands are observed in the 1560−1550 cm^{-1} region in unlabeled A_1^-/A_1 FTIR DS. Spectra obtained for ^2H-, ^{15}N-, and ^{13}C-labeled PS I all indicate that these bands are due to amide II modes. (2) A difference band at 1677−1674(+)/1666(−) cm^{-1} in ^1H A_1^-/A_1 FTIR DS is assigned to amide I modes. (3) A difference band at 1755(+)/1749(−) cm^{-1} in A_l^-/A_l FTIR DS is assigned to a 13^3 ester C═O mode of A_{0-A}. Thus the electrostatic field generated upon A_1^- formation impacts molecular groups that are >8 Å from A_1. (4) A negative band is observed at 1693 cm^{-1} that is most likely due to the 13^1 keto carbonyl group of A_{1-A}. (5) Positive bands at 1495 and 1414 cm^{-1} in the ^1H A_1^-/A_1 FTIR DS are assigned to C⋯O and C⋯C modes of A_1^-, respectively.

ACKNOWLEDGMENT

Whole cells of *S. 7002* were a gift from Donald Bryant at Pennsylvania State University. Thanks to Gaozhong Shen, Pennsylvania State University, for advice on growth and purification of PS I particles from *S. 7002*.

SUPPORTING INFORMATION AVAILABLE

Comparison of "early" and "late" time resolved FTIR DS with static FTIR DS. This material is available free of charge via the Internet at http://pubs.acs.org.

REFERENCES

1. Golbeck, J. H., and Bryant, D. (1991) Photosystem I, in *Current Topics in Bioenergetics*, Vol. 16, pp 83−175, Academic Press, New York.
2. Brettel, K. (1997) Electron transfer and arrangement of the redox cofactors in photosystem I, *Biochim. Biophys. Acta 1318*, 322−373.
3. Jordan, P., Fromme, P., Witt, H. T., Klukas, O., Saenger, W., and Krauss, N. (2001) Three-dimensional structure of cyanobacterial photosystem I at 2.5 angstrom resolution, *Nature 411*, 909−917.
4. Fromme, P., Jordan, P., and Krauss, N. (2001) Structure of photosystem I, *Biochim. Biophys. Acta 1507*, 5−31.
5. Guergova-Kuras, M., Boudreaux, B., Joliot, A., Joliot, P., and Redding, K. (2001) Evidence for two active branches for electron transfer in photosystem I, *Proc. Natl. Acad. Sci. U.S.A. 98*, 4437−4442.
6. Xu, W., Chitnis, P., Valieva, A., van der Est, A., Pushkar, Y. N., Krzystyniak, M., Teutloff, C., Zech, S. G., Bittl, R., Stehlik, D., Zybailov, B., Shen, G., and Golbeck, J. H. (2003) Electron transfer in cyanobacterial photosystem I: I. Physiological and spectroscopic characterization of site-directed mutants in a putative electron-transfer pathway from A_0 through A_1 to F_X, *J. Biol. Chem. 278*, 27864−27875.
7. Xu, W., Chitnis, P. R., Valieva, A., van der Est, A., Brettel, K., Guergova-Kuras, M., Pushkar, Y. N., Zech, S. G., Stehlik, D., Shen, G., Zybailov, B., and Golbeck, J. H. (2003) Electron transfer in cyanobacterial photosystem I: II. Determination of forward electron-transfer rates of site-directed mutants in a putative electron-transfer pathway from A_0 through A_1 to F_X, *J. Biol. Chem. 278*, 27876−27887.
8. Agalarov, R., and Brettel, K. (2003) Temperature dependence of biphasic forward electron transfer from the phylloquinone(s) A1 in photosystem I: only the slower phase is activated, *Biochim Biophys Acta 1604*, 7−12.
9. Schlodder, E., Falkenberg, K., Gergeleit, M., and Brettel, K. (1998) Temperature dependence of forward and reverse electron transfer from A_1^-, the reduced secondary electron acceptor in photosystem I, *Biochemistry 37*, 9466−9476.
10. Luneberg, J., Fromme, P., Jekow, P., and Schlodder, E. (1994) Spectroscopic Characterization of PS-I Core Complexes from Thermophilic *Synechococcus* Sp−Identical Reoxidation Kinetics of a(1)(−) before and after Removal of the Iron−Sulfur-Clusters F−a and F−B, *FEBS Lett. 338*, 197−202.
11. Uhmann, W., Becker, A., Taran, C., and Siebert, F. (1991) Time-Resolved FT-IR Absorption Spectroscopy Using a Step-Scan Interferometer, *Appl. Spectrosc. 45*, 390−397.
12. Hu, X., Frei, H., and Spiro, T. G. (1996) Nanosecond step-scan FTIR spectroscopy of hemoglobin: ligand recombination and protein conformational changes, *Biochemistry 35*, 13001−13005.
13. Hastings, G. (2001) Time-resolved step-scan Fourier transform infrared and visible absorption difference spectroscopy for the study of photosystem I, *Appl. Spectrosc. 55*, 894−900.
14. Plunkett, S. E., Chao, J. L., Tague, T. J., and Palmer, R. A. (1995) Time-Resolved Step-Scan Ft-Ir Spectroscopy of the Photodynamics of Carbonmonoxymyoglobin, *Appl. Spectrosc. 49*, 702−708.
15. Geux, N., and Peitsch, M. C. (1997) SWISS-MODEL and the Swiss-Pdb Viewer: An enivornment for comparative protein modeling, *Electrophoresis 18*, 2714−2723.

16. Shen, G., Zhao, J., Reimer, S. K., Antonkine, M. L., Cai, Q., Weiland, S. M., Golbeck, J. H., and Bryant, D. A. (2002) Assembly of photosystem I. I. Inactivation of the rubA gene encoding a membrane-associated rubredoxin in the cyanobacterium *Synechococcus* sp. PCC 7002 causes a loss of photosystem I activity, *J. Biol. Chem. 277*, 20343−20354.
17. Hastings, G., Reed, L., Lin, S., and Blankenship, R. (1995) Excited-state dynamics in photosystem I: effects of detergent and excitation wavelength, *Biophys. J. 69*, 2044−2055.
18. Hastings, G., Hoshina, S., Webber, A. and Blankenship, R. (1995) Universality of energy and electron-transfer processes in photosystem I, *Biochemistry 34*, 15512−15522.
19. Wang, R., Sivakumar, V., Johnson, T., and Hastings, G. (2004) FTIR Difference Spectroscopy In Combination With Isotope Labeling for Identification of the Carbonyl Modes of P700 and $P700^+$ in Photosystem I, *Biophys. J. 86*, 1061−1073.
20. Hastings, G., Ramesh, V. M., Wang, R., Sivakumar, V., and Webber, A. (2001) Primary donor photooxidation in photosystem I: a reevaluation of ($P700^{+-}$P700) Fourier transform infrared difference spectra, *Biochemistry 40*, 12943−12949.
21. Hastings, G., and Sivakumar, V. (2001) Time-resolved Fourier Transform Infrared Difference Spectroscopy for the Study of A_1 reduction in Intact Photosystem I, In *PS2001: 12th International Conference in Photosynthesis* (Critchley, C., Ed.) Abstr. S6-017, CSIRO Publishing, Melbourne, Australia.
22. Breton, J., Nabedryk, E., and Leibl, W. (1999) FTIR study of the primary electron donor of photosystem I (P700) revealing delocalization of the charge in P700(+) and localization of the triplet character in (3)P700, *Biochemistry 38*, 11585−11592.
23. Hastings, G., and Sivakumar, V. (2001) A Fourier transform infrared absorption difference spectrum associated with the reduction of A1 in photosystem I: are both phylloquinones involved in electron transfer? *Biochemistry 40*, 3681−3689.
24. Breton, J., Burie, J. R., Berthomieu, C., Berger, G., and Nabedryk, E. (1994) The binding sites of quinones in photosynthetic bacterial reaction centers investigated by light-induced FTIR difference spectroscopy: assignment of the Q_A vibrations in *Rhodobacter sphaeroides* using ^{18}O- or ^{13}C-labeled ubiquinone and vitamin K_1, *Biochemistry 33*, 4953−4965.
25. Hastings, G., Kleinherenbrink, F., Lin, S., McHugh, T., and Blankenship, R. (1994) Observation of the reduction and reoxidation of the primary electron acceptor in photosystem I, *Biochemistry 33*, 3193−3200.
26. Burie, J. R., Leibl, W., Nabedryk, E., and Breton, J. (1993) Step-Scan Ft-Ir Spectroscopy of Electron-Transfer in the Photosynthetic Bacterial Reaction-Center, *Appl. Spectrosc. 47*, 1401−1404.
27. Remy, A., and Gerwert, K. (2003) Coupling of light-induced electron transfer to proton uptake in photosynthesis, *Nat. Struct. Biol. 10*, 637−44.
28. Shen, G., Antonkine, M. L., van der Est, A., Vassiliev, I. R., Brettel, K., Bittl, R., Zech, S. G., Zhao, J., Stehlik, D., Bryant, D. A., and Golbeck, J. H. (2002) Assembly of photosystem I. II. Rubredoxin is required for the in vivo assembly of F(X) in *Synechococcus* sp. PCC 7002 as shown by optical and EPR spectroscopy, *J. Biol. Chem. 277*, 20355−20366.
29. Breton, J. (2001) Fourier transform infrared spectroscopy of primary electron donors in type I photosynthetic reaction centers, *Biochim. Biophys. Acta 1507*, 180−193.
30. Smith, B. C. (1999) *Infrared spectral interpretation: a systematic approach*, CRC Press, Boca Raton, FL.
31. Siebert, F., Mantele, W., and Kreutz, W. (1982) Evidence for the Protonation of Two Internal Carboxylic Groups during the Photocycle of Bacteriorhodopsin, *FEBS Lett. 141*, 82−87.
32. Nabedryk, E., Breton, J., Hienerwadel, R., Fogel, C., Mantele, W., Paddock, M. L. and Okamura, M. Y. (1995) Fourier transforms infrared difference spectroscopy of secondary quinone acceptor photoreduction in proton-transfer mutants of *Rhodobacter sphaeroides*, *Biochemistry 34*, 14722−14732.
33. Breton, J., Bibikova, M., Oesterhelt, D., and Nabedryk, E. (1999) Conformational heterogeneity of the bacteriopheophytin electron acceptor H_A in reaction centers from *Rhodopseudomonas viridis* revealed by Fourier transform infrared spectroscopy and site-directed mutagenesis, *Biochemistry 38*, 11541−11552.
34. Breton, J., and Nabedryk, E. (1998) Electrostatic Influence of Q_A and Q_B Reduction on the 10a-ester C═O Vibration in *Rp. viridis*, in *Photosynthesis: Mechanisms and Effects* (Garab, G., Ed.) Vol. II, pp 687−692, Kluwer Academic Publishers, Dordrecht and Boston.
35. Breton, J., and Nabedryk, E. (1995) Protein and Bacteriopheophytin Response to Q_A Reduction in Photosynthetic Bacterial Reaction Centers from *Rb. sphaeroides* and *Rp. viridis* Investigated by $^1H/^2H$ Exchange and Light-Induced FTIR Difference Spectroscopy, in *Photosynthesis: From Light to the Biosphere* (Mathis, P., Ed.) Vol. I, pp 395−400, Kluwer Academic Publishers, Dordrecht and Boston.
36. Breton, J., Nabedryk, E., Allen, J. P., and Williams, J. C. (1997) Electrostatic influence of Q_A reduction on the IR vibrational mode of the 10a-ester C═O of H_A demonstrated by mutations at residues Glu L104 and Trp L100 in reaction centers from *Rhodobacter sphaeroides*, *Biochemistry 36*, 4515−4525.
37. Brettel, K. (1988) Electron-Transfer from A_1 to an Iron−Sulfur Center with $t_{1/2}$ = 200 ns at Room-Temperature in Photosystem I. Characterization by Flash Absorption Spectroscopy, *FEBS Lett. 239*, 93−98.
38. Sivakumar, V., Wang, R., Johnson, T., and Hastings, G. (2004) A_1 Reduction in Intact Cyanobacterial Photosystem I Studied Using Time-resolved Step-scan Fourier Transform Infrared Difference Spectroscopy In Combination with Site Directed Mutagenesis and Quinone Exchange Experiments, in *Photosynthesis: Fundamental Aspects to Global Perspectives* (Carpentier, R., Ed.) Allen Press, Lawrence, KS (in press).
39. Grafton, A. K., Boesch, S. E., and Wheeler, R. A. (1997) Structures and properties of vitamin K and its radical anion predicted by a hybrid Hartree−Fock density functional method, *THEOCHEM−J. Mol. Struct. 392*, 1−11.
40. Grafton, A. K., and Wheeler, R. A. (1997) A comparison of the properties of various fused-ring quinones and their radical anions using Hartree−Fock and hybrid Hartree−Fock density functional methods, *J. Phys. Chem. A 101*, 7154−7166.
41. Barth, A. (2000) The infrared absorption of amino acid side chains, *Prog. Biophys. Mol. Biol. 74*, 141−173.
42. Bauscher, M., and Mantele, W. (1992) Electrochemical and Infrared-Spectroscopic Characterization of Redox Reactions of p-Quinones, *J. Phys. Chem. 96*, 11101−11108.
43. Breton, J., Boullais, C., Burie, J. R., Nabedryk, E., and Mioskowski, C. (1994) Binding sites of quinones in photosynthetic bacterial reaction centers investigated by light-induced FTIR difference spectroscopy: assignment of the interactions of each carbonyl of Q_A in *Rhodobacter sphaeroides* using site-specific ^{13}C-labeled ubiquinone, *Biochemistry 33*, 14378−14386.
44. Pushkar, Y., Golbeck, J., Stehlik, D., and Zimmermann, H. (2004) Asymmetric hydrogen-bonding of the quinone cofactor in Photosystem I probed by ^{13}C labeled naphthoquinones, *J. Phys. Chem. B 108*, 9439−9448.

BI0497493